

Tidal Evolution of Exoplanets

Alexandre C. M. Correia
University of Aveiro

Jacques Laskar
Paris Observatory

Tidal effects arise from differential and inelastic deformation of a planet by a perturbing body. The continuous action of tides modify the rotation of the planet together with its orbit until an equilibrium situation is reached. It is often believed that synchronous motion is the most probable outcome of the tidal evolution process, since synchronous rotation is observed for the majority of the satellites in the solar system. However, in the nineteenth century, Schiaparelli also assumed synchronous motion for the rotations of Mercury and Venus, and was later proven wrong. Rather, for planets in eccentric orbits, synchronous rotation is very unlikely. The rotation period and axial tilt of exoplanets is still unknown, but a large number of planets have been detected close to the parent star and should have evolved to a final equilibrium situation. Therefore, based on the well-studied cases in the solar system, we can make some predictions for exoplanets. Here we describe in detail the main tidal effects that modify the secular evolution of the spin and the orbit of a planet. We then apply our knowledge acquired from solar system situations to exoplanet cases. In particular, we will focus on two classes of planets, hot Jupiters (fluid) and super Earths (rocky with atmosphere).

1. INTRODUCTION

The occurrence on most open ocean coasts of high sea tide at about the time of the Moon's passage across the meridian long ago prompted the idea that Earth's satellite exerts an attraction on the water. The occurrence of a second high tide when the Moon is on the opposite meridian was a great puzzle, but the correct explanation of the tidal phenomena was given by Newton in *Philosophiae Naturalis Principia Mathematica*. Tides are a consequence of the lunar and solar gravitational forces acting in accordance with laws of mechanics. Newton realized that the tidal forces also must affect the atmosphere, but he assumed that the atmospheric tides would be too small to be detected, because changes in weather would introduce large irregular variations upon barometric measurements.

However, the semidiurnal oscillations of the atmospheric surface pressure has proven to be one of the most regular of all meteorological phenomena. It is readily detectable by harmonic analysis at any station in the world (e.g., Chapman and Lindzen, 1970). The main difference in respect to ocean tides is that atmospheric tides follow the Sun and not the Moon, as the atmosphere is essentially excited by solar heat. Even though tides of gravitational origin are present in the atmosphere, the thermal tides are more important as the pressure variations on the ground are more sensitive to the temperature gradients than to the gravitational ones.

The inner planets of the solar system as well as the majority of the main satellites present today a spin that is dif-

ferent from what is believed to have been the initial one (e.g., Goldreich and Soter, 1966; Goldreich and Peale, 1968). Planets and satellites are supposed to rotate much faster in the beginning, and any orientation of the spin axis may be allowed (e.g., Dones and Tremaine, 1993; Kokubo and Ida, 2007). However, tidal dissipation within the internal layers give rise to secular evolution of planetary spins and orbits. In the case of the satellites, spin and orbital evolution is mainly driven by tidal interactions with the central planet, whereas for the inner planets the main source of tidal dissipation is the Sun (in the case of Earth, tides raised by the Moon are also important).

Orbital and spin evolution cannot be dissociated because the total angular momentum must be conserved. As a consequence, a reduction in the rotation rate of a body implies an increment of the orbit semimajor axis and vice-versa. For instance, the Earth's rotation period is increasing about 2 ms/century (e.g., Williams, 1990), and the Moon is consequently moving away about 3.8 cm/yr (e.g., Dickey et al., 1994). On the other hand, Neptune's moon, Triton, and the martian moon, Phobos, are spiraling down into the planet, clearly indicating that the present orbits are not primordial, and may have undergone a long evolving process from a previous capture from a heliocentric orbit (e.g., Mignard, 1981; Goldreich et al., 1989; Correia, 2009). Both the Earth's Moon and Pluto's moon, Charon, have a significant fraction of the mass of their systems, and therefore could be classified as double planets rather than as satellites. The protoplanetary disk is unlikely to produce double-planet systems whose

origin seems to be due to a catastrophic impact of the initial planet with a body of comparable dimensions (e.g., *Canup and Asphaug*, 2001; *Canup*, 2005). The resulting orbits after collision are most likely eccentric, but the present orbits are almost circular, suggesting that tidal evolution subsequently occurred.

The ultimate stage for tidal evolution corresponds to the synchronous rotation, a configuration where the rotation rate coincides with the orbital mean motion, since synchronous equilibrium corresponds to the minimum of dissipation of energy. However, when the eccentricity is different from zero, some other configurations are possible, such as the 3/2 spin-orbit resonance observed for the planet Mercury (*Colombo*, 1965; *Goldreich and Peale*, 1966; *Correia and Laskar*, 2004) or the chaotic rotation of Hyperion (*Wisdom et al.*, 1984). When a dense atmosphere is present, thermal atmospheric tides may counterbalance the gravitational tidal effect and nonresonant equilibrium configurations are also possible, as illustrated by the retrograde rotation of Venus (*Correia and Laskar*, 2001). Additional effects may also contribute to the final evolution of the spin, such as planetary perturbations or core-mantle friction.

Despite the proximity of Mercury and Venus to Earth, the determination of their rotational periods has only been achieved in the second half of the twentieth century, when it became possible to use radar ranging on the planets (*Pettengill and Dyce*, 1965; *Goldstein*, 1964; *Carpenter*, 1964). We thus do not expect that it will be easy to observe the rotation of the recently discovered exoplanets. Nevertheless, many of the exoplanets are close to their host star, and we can assume that exoplanets' spin and orbit have already undergone enough dissipation and evolved into a final equilibrium possibility. An identical assumption has been done before for Mercury and Venus by *Schiaparelli* (1889), who made predictions for their rotations based on *Darwin's* work (1880). *Schiaparelli's* predictions were later proven to be wrong, but were nevertheless much closer to the true rotation periods than most values derived from observations in the two previous centuries. Like *Schiaparelli*, we may dare to establish predictions for the rotation periods of some already known exoplanets. We hope that the additional knowledge that we gained from a better understanding of the rotation of Mercury and Venus will help us to be at least as close to reality as *Schiaparelli*. Indeed, observations also show that many of the exoplanets have highly eccentric orbits. In some cases eccentricities larger than 0.9 are found (e.g., *Naef et al.*, 2001; *Jones et al.*, 2006; *Tamuz et al.*, 2008), which introduces the possibility of a wide variety of final tidal equilibrium positions, different from what we observe around the Sun.

In this chapter we will describe the tidal effects that modify the secular evolution of the spin and orbit of a planet. We then apply our knowledge acquired from solar system situations to exoplanet cases. In particular, we will focus on two classes of planets, hot Jupiters (fluid) and super Earths (rocky), which are close to the star and therefore more susceptible to having arrived in a final equilibrium situation.

2. MODEL DESCRIPTION

We will first omit the tidal effects, and describe the spin motion of the planet in a conservative framework. The motion equations will be obtained from a Hamiltonian formalism (e.g., *Goldstein*, 1950) of the total gravitational energy of the planet (section 2.1). Gravitational tides (section 2.2) and thermal atmospheric tides (section 2.3) will be described later. We also discuss the impact of spin-orbit resonances (section 2.4) and planetary perturbations (section 2.5).

2.1. CONSERVATIVE MOTION

The planet is considered here as a rigid body with mass m and moments of inertia $A \leq B < C$, supported by the reference frame $(\mathbf{I}, \mathbf{J}, \mathbf{K})$, fixed with respect to the planet's figure. Let \mathbf{L} be the total rotational angular momentum and $(\mathbf{i}, \mathbf{j}, \mathbf{k})$ a reference frame linked to the orbital plane (where \mathbf{k} is the normal for this plane). As we are interested in the long-term behavior of the spin axis, we merge the axis of figure \mathbf{K} with the direction of the angular momentum \mathbf{L} . Indeed, the average of \mathbf{K} coincides with \mathbf{L}/L up to J^2 , where $\cos J = \mathbf{L} \cdot \mathbf{K}$ (*Boué and Laskar*, 2006). J is extremely small for large rocky planets ($J \approx 7 \times 10^{-7}$ for Earth), being even smaller for Jupiter-like planets that behave as fluids. The angle between \mathbf{K} and \mathbf{k} is the obliquity, ε , and thus, $\cos \varepsilon = \mathbf{k} \cdot \mathbf{K}$ (Fig. 1).

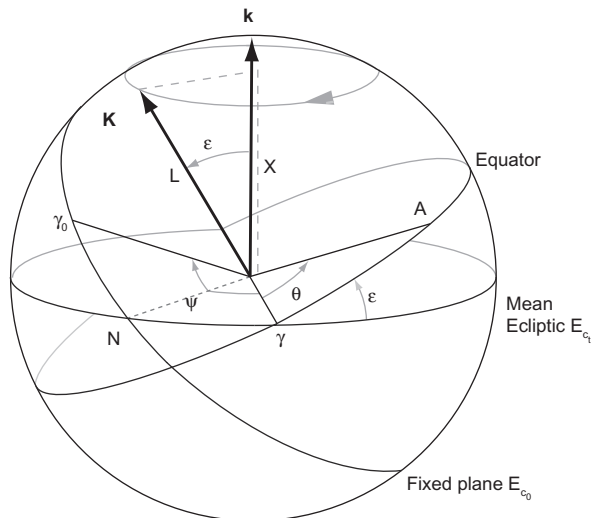


Fig. 1. Andoyer's canonical variables. \mathbf{L} is the projection of the total rotational angular momentum vector \mathbf{L} on the principal axis of inertia \mathbf{K} , and \mathbf{X} the projection of the angular momentum vector on the normal to the orbit (or ecliptic) \mathbf{k} . The angle between the equinox of date γ and a fixed point of the equator \mathbf{A} is the hour angle θ , and $\psi = \gamma \mathbf{N} + \mathbf{N} \gamma_0$ is the general precession angle. The direction of γ_0 is on a fixed plane E_{c0} , while γ is on the mean orbital (or ecliptic) E_{ct} of date t .

The Hamiltonian of the motion can be written using canonical Andoyer's action variables (L , X) and their conjugate angles (θ , $-\psi$) (Andoyer, 1923; Kinoshita, 1977). $L = \mathbf{L} \cdot \mathbf{K} = C\omega$ is the projection of the angular momentum on the C axis, with rotation rate $\omega = \dot{\theta} - \dot{\psi} \cos \epsilon$, and $X = \mathbf{L} \cdot \mathbf{k}$ is the projection of the angular momentum on the normal to the ecliptic; θ is the hour angle between the equinox of date and a fixed point of the equator, and ψ is the general precession angle, an angle that simultaneously accounts for the precession of the spin axis and the orbit (Fig. 1).

2.1.1. Gravitational potential. The gravitational potential V (energy per unit mass) generated by the planet at a generic point of the space \mathbf{r} , expanded in degree two of R/r , where R is the planet's radius, is given by (e.g., Tisserand, 1891; Smart, 1953)

$$\begin{aligned} V(\mathbf{r}) = & -\frac{Gm}{r} + \frac{G(B-A)}{r^3} P_2(\hat{\mathbf{r}} \cdot \mathbf{J}) \\ & + \frac{G(C-A)}{r^3} P_2(\hat{\mathbf{r}} \cdot \mathbf{K}) \end{aligned} \quad (1)$$

where $\hat{\mathbf{r}} = \mathbf{r}/r$, G is the gravitational constant, and $P_2(x) = (3x^2 - 1)/2$ are the Legendre polynomials of degree two. The potential energy U when orbiting a central star of mass m_\star is then

$$U = m_\star V(r) \quad (2)$$

For a planet evolving in a nonperturbed Keplerian orbit, we write

$$\hat{\mathbf{r}} = \cos(\varpi + v)\mathbf{i} + \sin(\varpi + v)\mathbf{j} \quad (3)$$

where ϖ is the longitude of the perihelion and v the true anomaly (see chapter by Murray and Correia). Thus, transforming the body equatorial frame ($\mathbf{I}, \mathbf{J}, \mathbf{K}$) into the orbital frame ($\mathbf{i}, \mathbf{j}, \mathbf{k}$), we obtain (Fig. 1)

$$\begin{cases} \hat{\mathbf{r}} \cdot \mathbf{J} = -\cos w \sin \theta + \sin w \cos \theta \cos \epsilon \\ \hat{\mathbf{r}} \cdot \mathbf{K} = -\sin w \sin \epsilon \end{cases} \quad (4)$$

where $w = \varpi + \psi + v$ is the true longitude to date. The expression for the potential energy (equation (2)) becomes (e.g., Correia, 2006)

$$\begin{aligned} U = & -\frac{Gmm_\star}{r} + \frac{GCm_\star}{r^3} E_d P_2(\sin w \sin \epsilon) \\ & - \frac{3Gm_\star}{8r^3} (B-A) F(\theta, w, \epsilon) \end{aligned} \quad (5)$$

where

$$\begin{aligned} F(\theta, w, \epsilon) = & 2 \cos(2\theta - 2w) \cos^4\left(\frac{\epsilon}{2}\right) \\ & + 2 \cos(2\theta + 2w) \sin^4\left(\frac{\epsilon}{2}\right) + \cos(2\theta) \sin^2 \epsilon \end{aligned} \quad (6)$$

and

$$E_d = \frac{C - \frac{1}{2}(A+B)}{C} = \frac{k_f R^5}{3GC} \omega^2 + \delta E_d \quad (7)$$

where E_d is the dynamical ellipticity, and k_f is the fluid Love number (pertaining to a perfectly fluid body with the same mass distribution as the actual planet). The first part of E_d (equation (7)) corresponds to the flattening in hydrostatic equilibrium (Lambeck, 1980), and δE_d to the departure from this equilibrium.

2.1.2. Averaged potential. Since we are only interested in the study of the long-term motion, we will average the potential energy U over the rotation angle θ and the mean anomaly M

$$\bar{U} = \frac{1}{4\pi^2} \int_0^{2\pi} \int_0^{2\pi} U dM d\theta \quad (8)$$

However, when the rotation frequency $\omega \approx \dot{\theta}$ and the mean motion $n = \dot{M}$ are close to resonance ($\omega \approx pn$, for a semi-integer value p), the terms with argument $2(\theta - pM)$ vary slowly and must be retained in the expansions (e.g., Murray and Dermott, 1999)

$$\frac{\cos(2\theta)}{r^3} = \frac{1}{a^3} \sum_{p=-\infty}^{+\infty} G(p, e) \cos 2(\theta - pM) \quad (9)$$

and

$$\frac{\cos(2\theta - 2w)}{r^3} = \frac{1}{a^3} \sum_{p=-\infty}^{+\infty} H(p, e) \cos 2(\theta - pM) \quad (10)$$

where a and e are the semimajor axis and the eccentricity of the planet's orbit, respectively. The functions $G(p, e)$ and $H(p, e)$ can be expressed in power series in e (Table 1). The averaged nonconstant part of the potential \bar{U} becomes

$$\begin{aligned} \frac{\bar{U}}{C} = & -\alpha \frac{\omega x^2}{2} - \frac{\beta}{4} \left[(1-x^2) G(p, e) \cos 2(\theta - pM) \right. \\ & + \frac{(1+x)^2}{2} H(p, e) \cos 2(\theta - pM - \phi) \\ & \left. + \frac{(1-x)^2}{2} H(-p, e) \cos 2(\theta - pM + \phi) \right] \end{aligned} \quad (11)$$

where $x = X/L = \cos \epsilon$, $\phi = \varpi + \psi$

$$\alpha = \frac{3Gm_\star}{2a^3(1-e^2)^{3/2}} \frac{E_d}{\omega} \approx \frac{3}{2} \frac{n^2}{\omega} (1-e^2)^{-3/2} E_d \quad (12)$$

is the “precession constant” and

$$\beta = \frac{3Gm_\star}{2a^3} \frac{B-A}{C} \approx \frac{3}{2} n^2 \frac{B-A}{C} \quad (13)$$

TABLE 1. Coefficients of G (p,e) and H (p,e) to e^4 .

p	G(p,e)			H(p,e)		
-1		$\frac{9}{4}e^2$	+	$\frac{7}{4}e^4$		$\frac{1}{24}e^4$
-1/2		$\frac{3}{2}e$	+	$\frac{27}{16}e^3$		$\frac{1}{48}e^3$
0	1	+	$\frac{3}{2}e^2$	+	$\frac{15}{8}e^4$	0
1/2		$\frac{3}{2}e$	+	$\frac{27}{16}e^3$	-	$\frac{1}{2}e$
1		$\frac{9}{4}e^2$	+	$\frac{7}{4}e^4$	1	-
3/2			$\frac{53}{16}e^3$		$\frac{7}{2}e$	-
2			$\frac{77}{16}e^4$		$\frac{17}{2}e^2$	-
5/2					$\frac{845}{48}e^3$	
3						$\frac{533}{16}e^4$

The exact expression of the coefficients is given by $G(p,e) = \frac{1}{\pi} \int_0^\pi \left(\frac{a}{r}\right)^3 \exp(i2pM) dM$ and $H(p,e) = \frac{1}{\pi} \int_0^\pi \left(\frac{a}{r}\right)^3 \exp(i2v) \exp(i2pM) dM$.

For nonresonant motion, that is, when $(B-A)/C \approx 0$ (e.g., gaseous planets) or $|\omega| \gg pn$, we can simplify expression (11) as

$$\frac{\bar{U}}{C} = -\alpha \frac{\omega x^2}{2} \quad (14)$$

2.1.3. Equations of motion. The Andoyer variables (L , θ) and (X , $-\psi$) are canonically conjugated and thus (e.g., Goldstein, 1950; Kinoshita, 1977)

$$\frac{dL}{dt} = -\frac{\partial \bar{U}}{\partial \theta}, \quad \frac{dX}{dt} = \frac{\partial \bar{U}}{\partial \psi}, \quad \frac{d\psi}{dt} = -\frac{\partial \bar{U}}{\partial X} \quad (15)$$

Andoyer's variables do not give a clear view of the spin variations, despite their practical use. Since $\omega = L/C$ and $\cos \epsilon = x = X/L$ the spin variations can be obtained as

$$\frac{d\omega}{dt} = -\frac{\partial}{\partial \theta} \left(\frac{\bar{U}}{C} \right), \quad \frac{d\psi}{dt} = -\frac{1}{\omega} \frac{\partial}{\partial x} \left(\frac{\bar{U}}{C} \right) \quad (16)$$

and

$$\begin{aligned} \frac{dx}{dt} &= -\frac{1}{L} \left(\frac{X}{L} \frac{dL}{dt} - \frac{dX}{dt} \right) \\ &= \frac{1}{\omega} \left[x \frac{\partial}{\partial \theta} + \frac{\partial}{\partial \psi} \right] \left(\frac{\bar{U}}{C} \right) \end{aligned} \quad (17)$$

For nonresonant motion, we get from equation (14)

$$\frac{d\omega}{dt} = \frac{dx}{dt} = 0 \quad \text{and} \quad \frac{d\psi}{dt} = \alpha x \quad (18)$$

The spin motion reduces to the precession of the spin vector about the normal to the orbital plane with rate αx .

2.2. Gravitational Tides

Gravitational tides arise from differential and inelastic deformations of the planet due to the gravitational effect of a perturbing body (which can be the central star or a satellite). Tidal contributions to the planet evolution are based on a very general formulation of the tidal potential, initiated by Darwin (1880). The attraction of a body with mass m_\star at a distance r from the center of mass of the planet can be expressed as the gradient of a scalar potential V' , which is a sum of Legendre polynomials (e.g., Kaula, 1964; Efroimsky and Williams, 2009)

$$V' = \sum_{l=2}^{\infty} V'_l = -\frac{Gm_\star}{r} \sum_{l=2}^{\infty} \left(\frac{r'}{r} \right)^l P_l(\cos S) \quad (19)$$

where r' is the radial distance from the planet's center, and S the angle between \mathbf{r} and \mathbf{r}' . The distortion of the planet by the potential V' gives rise to a tidal potential

$$V_g = \sum_{l=2}^{\infty} (V_g)_l \quad (20)$$

where $(V_g)_l = k_l V'_l$ at the planet's surface and k_l is the Love number for potential (Fig. 2). Typically, $k_2 \sim 0.25$ for Earth-like planets, and $k_2 \sim 0.40$ for giant planets (Yoder, 1995). Since the tidal potential $(V_g)_l$ is an l th degree harmonic, it is a solution of a Dirichlet problem, and exterior to the planet it must be proportional to r^{-l-1} (e.g., Abramowitz and Stegun, 1972; Lambeck, 1980). Furthermore, as upon the surface $r' = R \ll r$, we can retain in expression (20) only the first term, $l = 2$

$$V_g = -k_2 \frac{Gm_\star}{R} \left(\frac{R}{r} \right)^3 \left(\frac{R}{r'} \right)^3 P_2(\cos S) \quad (21)$$

In general, imperfect elasticity will cause the phase angle of V_g to lag behind that of V' (Kaula, 1964) by an angle $\delta_g(\sigma)$ such that

$$2\delta_g(\sigma) = \sigma \Delta t_g(\sigma) \quad (22)$$

$\Delta t_g(\sigma)$ being the time lag associated with the tidal frequency σ (a linear combination of the inertial rotation rate ω and the mean orbital motion n) (Fig. 3).

2.2.1. Equations of motion. Expressing the tidal potential given by expression (21) in terms of Andoyer angles (θ, ψ) , we can obtain the contribution to the spin evolution from expression (15) using $U_g = m'V_g$ at the place of \bar{U} , where m' is the mass of the interacting body. As we are interested here in the study of the secular evolution of the spin, we also average U_g over the periods of mean anomaly and longitude of the perihelion of the orbit. When the interacting body is the same as the perturbing body ($m' = m_\star$), we obtain

$$\frac{d\omega}{dt} = -\frac{Gm_\star^2 R^5}{Ca^6} \sum_{\sigma} b_g(\sigma) \Omega_{\sigma}^g(x, e) \quad (23)$$

$$\frac{de}{dt} = -\frac{Gm_\star^2 R^5}{Ca^6} \frac{\sin e}{\omega} \sum_{\sigma} b_g(\sigma) E_{\sigma}^g(x, e) \quad (24)$$

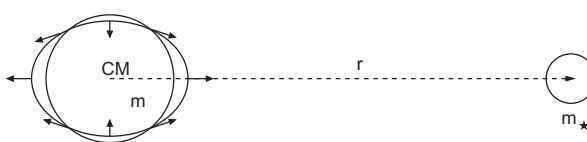


Fig. 2. Gravitational tides. The difference between the gravitational force exerted by the mass m on a point of the surface and the center of mass is schematized by the arrows. The planet will deform following the equipotential of all present forces.

where the coefficients $\Omega_{\sigma}^g(x, e)$ and $E_{\sigma}^g(x, e)$ are polynomials in the eccentricity (Kaula, 1964). When the eccentricity is small, we can neglect the terms in e^2 , and we have

$$\begin{aligned} \Sigma_{\sigma} b_{\tau}(\sigma) \Omega_{\sigma}^{\tau} &= b_{\tau}(\omega) \frac{3}{4} x^2 (1-x^2) \\ &+ b_{\tau}(\omega-2n) \frac{3}{16} (1+x)^2 (1-x^2) \\ &+ b_{\tau}(\omega+2n) \frac{3}{16} (1-x)^2 (1-x^2) \\ &+ b_{\tau}(2\omega) \frac{3}{8} (1+x^2)^2 \\ &+ b_{\tau}(2\omega-2n) \frac{3}{32} (1+x)^4 \\ &+ b_{\tau}(2\omega+2n) \frac{3}{32} (1-x)^4 \end{aligned} \quad (25)$$

and

$$\begin{aligned} \Sigma_{\sigma} b_{\tau}(\sigma) E_{\sigma}^{\tau} &= b_{\tau}(2n) \frac{9}{16} (1-x^2) \\ &+ b_{\tau}(\omega) \frac{3}{4} x^3 \\ &- b_{\tau}(\omega-2n) \frac{3}{16} (1+x)^2 (2-x) \\ &+ b_{\tau}(\omega+2n) \frac{3}{16} (1-x)^2 (2+x) \\ &+ b_{\tau}(2\omega) \frac{3}{8} x (1-x^2) \\ &- b_{\tau}(2\omega-2n) \frac{3}{32} (1+x)^3 \end{aligned} \quad (26)$$

The coefficients $b_{\tau}(\sigma)$ are related to the dissipation of the mechanical energy of tides in the planet's interior, responsible for the time delay $\Delta t_g(\sigma)$ between the position of “maximal tide” and the substellar point. They are related to the phase lag $\delta_g(\sigma)$ as

$$b_g(\sigma) = k_2 \sin 2\delta_g(\sigma) = k_2 \sin(\sigma \Delta t_g(\sigma)) \quad (27)$$

where $\tau = g$ for gravitational tides. Dissipation equations (23) and (24) must be invariant under the change (ω, x) by $(-\omega, -x)$, which imposes that $b(\sigma) = -b(-\sigma)$, that is, $b(\sigma)$ is an odd function of σ . Although mathematically equivalent, the couples (ω, x) and $(-\omega, -x)$ correspond to two different physical situations (Correia and Laskar, 2001).

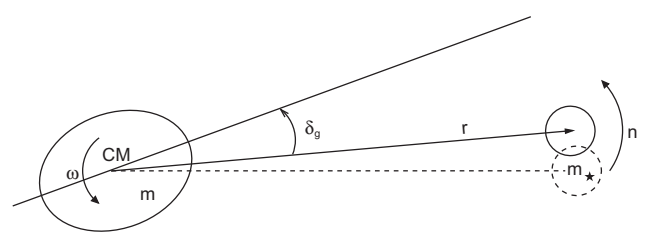


Fig. 3. Phase lag for gravitational tides. The tidal deformation takes a delay time Δt_g to attain the equilibrium. During the time Δt_g , the planet turns by an angle $\omega \Delta t_g$ and the star by $n \Delta t_g$. For $e = 0$, the bulge phase lag is given by $\delta_g \approx (\omega - n) \Delta t_g$.

The tidal potential given by expression (21) can also be directly used to compute the orbital evolution due to tides. Indeed, it can be seen as a perturbation of the gravitational potential (equation (1)), and the contributions to the orbit are computed using Lagrange planetary equations (e.g., *Brouwer and Clemence*, 1961; *Kaula* 1964)

$$\frac{da}{dt} = \frac{2}{mna^7} \frac{\partial U}{\partial M} \quad (28)$$

$$\frac{de}{dt} = \frac{\sqrt{1-e^2}}{mna^2 e} \left[\sqrt{1-e^2} \frac{\partial U}{\partial M} - \frac{\partial U}{\partial \omega} \right] \quad (29)$$

We then find for the orbital evolution of the planet

$$\frac{da}{dt} = -\frac{6Gm_\star^2 R^5}{mna^7} \sum_{\sigma} b_g(\sigma) A_{\sigma}^g(x, e) \quad (30)$$

$$\frac{de}{dt} = -e \frac{3Gm_\star^2 R^5}{mna^8} \sum_{\sigma} b_g(\sigma) E_{\sigma}^g(x, e) \quad (31)$$

where the coefficients $A_{\sigma}^g(x, e)$ and $E_{\sigma}^g(x, e)$ are again polynomials in the eccentricity. When the eccentricity is small, we can neglect the terms in e^2 , and we have

$$\begin{aligned} \Sigma_{\sigma} b_{\tau}(\sigma) A_{\sigma}^{\tau} &= b_{\tau}(2n) \frac{9}{16} (1-x^2)^2 \\ &- b_{\tau}(\omega-2n) \frac{3}{8} (1-x^2)(1+x)^2 \\ &+ b_{\tau}(\omega+2n) \frac{3}{8} (1-x^2)(1-x)^2 \\ &- b_{\tau}(2\omega-2n) \frac{3}{32} (1+x)^4 \\ &+ b_{\tau}(2\omega+2n) \frac{3}{32} (1-x)^4 \end{aligned} \quad (32)$$

and

$$\begin{aligned} \Sigma_{\sigma} b_{\tau}(\sigma) E_{\sigma}^{\tau} &= b_{\tau}(n) \frac{9}{128} (5x^2-1)(7x^2-3) \\ &- b_{\tau}(2n) \frac{9}{32} (1-x^2)^2 \\ &+ b_{\tau}(3n) \frac{441}{128} (1-x^2)^2 \\ &- b_{\tau}(\omega-n) \frac{3}{64} (5x-1)(7x+1)(1-x^2) \\ &+ b_{\tau}(\omega+n) \frac{3}{64} (5x+1)(7x-1)(1-x^2) \\ &+ b_{\tau}(\omega-2n) \frac{3}{16} (1-x^2)(1+x)^2 \\ &- b_{\tau}(\omega+2n) \frac{3}{16} (1-x^2)(1-x)^2 \\ &- b_{\tau}(\omega-3n) \frac{3}{64} (1-x^2)(1+x)^2 \\ &+ b_{\tau}(\omega+3n) \frac{3}{64} (1-x^2)(1-x)^2 \\ &- b_{\tau}(2\omega-n) \frac{3}{256} (5x-7)(7x-5)(1+x)^2 \\ &+ b_{\tau}(2\omega+n) \frac{3}{256} (5x+7)(7x+5)(1-x)^2 \\ &+ b_{\tau}(2\omega-2n) \frac{3}{64} (1+x)^4 \\ &- b_{\tau}(2\omega+2n) \frac{3}{64} (1-x)^4 \\ &- b_{\tau}(2\omega-3n) \frac{147}{256} (1+x)^4 \\ &+ b_{\tau}(2\omega+3n) \frac{147}{256} (1-x)^4 \end{aligned} \quad (33)$$

2.2.2. Dissipation models. The dissipation of the mechanical energy of tides in the planet's interior is responsible for the phase lag $\delta(\sigma)$. A commonly used dimensionless measure of tidal damping is the quality factor Q (*Munk and MacDonald*, 1960), defined as the inverse of the "specific" dissipation and related to the phase lags by

$$Q(\sigma) = \frac{2\pi E}{\Delta E} = \cot 2\delta(\sigma) \quad (34)$$

where E is the total tidal energy stored in the planet, and ΔE the energy dissipated per cycle. We can rewrite expression (27) as

$$b_g(\sigma) = \frac{k_2 \text{sign}(\sigma)}{\sqrt{Q^2(\sigma)+1}} \approx \text{sign}(\sigma) \frac{k_2}{Q(\sigma)} \quad (35)$$

The present Q value for the planets in the solar system can be estimated from orbital measurements, but as the rheology of the planets is poorly known, the exact dependence of $b_g(\sigma)$ on the tidal frequency σ is unknown. Many different authors have studied the problem and several models for $b_g(\sigma)$ have been developed so far, from the simplest to the more complex (for a review see *Efroimsky and Williams*, 2009). The huge problem in declaring one model to be more valid than the others is the difficulty of comparing theoretical results with the observations, as the effect of tides are very small and can only be efficiently detected after long periods of time. Therefore, here we will only describe a few simplified models that are commonly used:

The viscoelastic model. *Darwin* (1908) assumed that the planet behaves like a Maxwell solid, i.e., the planet responds to stresses like a massless, damped harmonic oscillator. It is characterized by a rigidity (or shear modulus) μ_e and by a viscosity v_e . A Maxwell solid behaves like an elastic solid over short timescales, but flows like a fluid over long periods of time. This behavior is also known as elasticoviscosity. For a constant density ρ , we have

$$b_g(\sigma) = k_f \frac{\tau_b - \tau_a}{1 + (\tau_b \sigma)^2} \sigma \quad (36)$$

where k_f is the fluid Love number (equation (7)). $\tau_a = v_e / \mu_e$ and $\tau_b = \tau_a(1 + 19\mu_e R/2Gmp)$ are time constants for the damping of gravitational tides.

The viscoelastic model is a realistic approximation of the planet's deformation with the tidal frequency (e.g., *Escribano et al.*, 2008). However, when substituting expression (36) into the dynamical equations (23) and (24) we get an infinite sum of terms, which is not practical. As a consequence, simplified versions of the viscoelastic model for specific values of the tidal frequency σ are often used. For instance, when σ is small, $(\tau_b \sigma)^2$ can be neglected in expression (36) and $b_g(\sigma)$ becomes proportional to σ .

The viscous or linear model. In the viscous model, it is assumed that the response time delay to the perturbation

is independent of the tidal frequency, i.e., the position of the “maximal tide” is shifted from the substellar point by a constant time lag Δt_g (*Mignard*, 1979, 1980). As we usually have $\sigma \Delta t_g \ll 1$, the viscous model becomes linear

$$b_g(\sigma) = k_2 \sin(\sigma \Delta t_g) \approx k_2 \sigma \Delta t_g \quad (37)$$

The viscous model is a particular case of the viscoelastic model and is specially adapted to describe the behavior of planets in slow rotating regimes ($\omega \sim n$).

The constant-Q model. Since for Earth, Q changes by less than an order of magnitude between the Chandler wobble period (about 440 d) and seismic periods of a few seconds (*Munk and MacDonald*, 1960), it is also common to treat the specific dissipation as independent of frequency. Thus

$$b_g(\sigma) = \text{sign}(\sigma) k_2 / Q \quad (38)$$

The constant-Q model can be used for periods of time where the tidal frequency does not change much, as is the case for fast rotating planets. However, for long-term evolutions and slow-rotating planets, the constant-Q model is not appropriate as it gives rise to discontinuities for $\sigma = 0$.

2.2.3. Consequences for the spin. Although both linear and constant models have some limitations, for reasons of simplicity they are the most widely used in literature. The linear model nevertheless has an important advantage over the constant model: It is appropriate to describe the behavior of the planet near the equilibrium positions, since the linear model closely follows the realistic viscoelastic model for slow rotation rates. The equations of motion can also be expressed in an elegant way, so we will adopt the viscous model for the remainder of this chapter, without loss of generality concerning the main consequences of tidal effects.

Using the approximation (37) in expressions (23) and (24), we simplify the spin equations as (*Correia and Laskar*, 2010, Appendix B)

$$\dot{\omega} = -\frac{Kn}{C} \left(f_1(e) \frac{1 + \cos^2 \epsilon}{2} \frac{\omega}{n} - f_2(e) \cos \epsilon \right) \quad (39)$$

and

$$\dot{\epsilon} \approx \frac{Kn}{C\omega} \sin \epsilon \left(f_1(e) \cos \epsilon \frac{\omega}{2n} - f_2(e) \right) \quad (40)$$

where

$$f_1(e) = \frac{1 + 3e^2 + 3e^4/8}{(1 - e^2)^{9/2}} \quad (41)$$

$$f_2(e) = \frac{1 + 15e^2/2 + 45e^4/8 + 5e^6/16}{(1 - e^2)^6} \quad (42)$$

and

$$K = \Delta t \frac{3k_2 G m_*^2 R^5}{a^6} \quad (43)$$

Because of the factor $1/\omega$ in the magnitude of the obliquity variations (equation (40)), for an initial fast-rotating planet the timescale for the obliquity evolution will be longer than the timescale for the rotation rate evolution (equation (39)). As a consequence, it is to be expected that the rotation rate reaches an equilibrium value earlier than the obliquity. For a given obliquity and eccentricity, the equilibrium rotation rate, obtained when $\dot{\omega} = 0$, is then attained (see Fig. 4) for

$$\frac{\omega_e}{n} = \frac{f_2(e)}{f_1(e)} \frac{2 \cos \epsilon}{1 + \cos^2 \epsilon} \quad (44)$$

Replacing the previous equation in the expression for obliquity variations (equation (40)), we find

$$\dot{\epsilon} \approx -\frac{Kn}{C\omega} f_2(e) \frac{\sin \epsilon}{1 + \cos^2 \epsilon} \quad (45)$$

We then conclude that the obliquity can only decrease by tidal effect, since $\dot{\epsilon} \leq 0$, and the final obliquity always tends to zero.

2.2.4. Consequences for the orbit. As for the spin, the semimajor axis and the eccentricity evolution can be obtained using approximation (37) in expressions (32) and (33), respectively (*Correia*, 2009)

$$\dot{a} = \frac{2K}{ma} \left(f_2(e) \cos \epsilon \frac{\omega}{n} - f_3(e) \right) \quad (46)$$

and

$$\dot{e} = \frac{9K}{ma^2} \left(\frac{11}{18} f_4(e) \cos \epsilon \frac{\omega}{n} - f_5(e) \right) e \quad (47)$$

where

$$f_3(e) = \frac{1 + 31e^2/2 + 255e^4/8 + 185e^6/16 + 25e^8/64}{(1 - e^2)^{15/2}} \quad (48)$$

$$f_4(e) = \frac{1 + 3e^2/2 + e^4/8}{(1 - e^2)^5} \quad (49)$$

$$f_5(e) = \frac{1 + 15e^2/4 + 15e^4/8 + 5e^6/64}{(1 - e^2)^{13/2}} \quad (50)$$

The ratio between orbital and spin evolution timescales is roughly given by $C/(ma^2) \ll 1$, meaning that the spin achieves an equilibrium position much faster than the orbit.

Replacing the equilibrium rotation rate (equation (44)) with $\varepsilon = 0$ (for simplicity) in equations (46) and (47) gives

$$\dot{a} = -\frac{7K}{ma} f_6(e) e^2 \quad (51)$$

$$\dot{e} = -\frac{7K}{2ma^2} f_6(e) (1-e^2) e^2 \quad (52)$$

where $f_6(e) = (1 + 45e^2/14 + 8e^4 + 685e^6/224 + 255e^8/448 + 25e^{10}/1792)(1-e^2)^{-15/2}/(1 + 3e^2 + 3e^4/8)$. Thus, we always have $\dot{a} \leq 0$ and $\dot{e} \leq 0$, and the final eccentricity is zero. Another consequence is that the quantity $a(1-e^2)$ is conserved (equation (101)). The final equilibrium semimajor axis is then given by

$$a_f = a(1-e^2) \quad (53)$$

which is a natural consequence of the orbital angular momentum conservation (since the rotational angular momentum of the planet is much smaller). Notice, however, that once the equilibrium semimajor axis a_f is attained, the tidal effects on the star cannot be neglected, and they govern the future evolution of the planet's orbit.

2.3. Thermal Atmospheric Tides

The differential absorption of the solar heat by the planet's atmosphere gives rise to local variations of temperature and consequently to pressure gradients. The mass of the atmosphere is then permanently redistributed, adjusting for an equilibrium position. More precisely, the particles of the atmosphere move from the high-temperature zone (at the substellar point) to the low-temperature areas. Indeed, observations on Earth show that the pressure redistribution

is essentially a superposition of two pressure waves (see Chapman and Lindzen, 1970): a daily (or diurnal) tide of small amplitude (the pressure is minimal at the substellar point and maximal at the antipode) and a strong half-daily (semidiurnal) tide (the pressure is minimal at the substellar point and at the antipode) (Fig. 5).

The gravitational potential generated by all the particles in the atmosphere at a generic point of the space \mathbf{r} is given by

$$V_a = -G \int_{(\mathcal{M})} \frac{d\mathcal{M}}{|\mathbf{r} - \mathbf{r}'|} \quad (54)$$

where $\mathbf{r}' = (r', \theta', \phi')$ is the position of the atmosphere mass element $d\mathcal{M}$ with density $\rho_a(\mathbf{r}')$ and

$$d\mathcal{M} = \rho_a(\mathbf{r}') r'^2 \sin \theta' dr' d\theta' d\phi' \quad (55)$$

Assuming that the radius of the planet is constant and that the height of the atmosphere can be neglected, we approximate expression (55) as

$$d\mathcal{M} = \frac{R^2}{g} p_s(\theta', \phi') \sin \theta' d\theta' d\phi' \quad (56)$$

where g is the mean surface gravity acceleration and p_s the surface pressure, which depends on the stellar insolation. Thus, p_s depends on S , the angle between the direction of the Sun and the normal to the surface

$$p_s(\theta', \phi') = p_s(S) = \sum_{l=0}^{+\infty} \tilde{p}_l P_l(\cos S) \quad (57)$$

where P_l are the Legendre polynomials on the order of l and \tilde{p}_l its coefficients. Developing also $|\mathbf{r} - \mathbf{r}'|^{-l}$ in Legendre polynomials we rewrite expression (54) as

$$V_a = -\frac{1}{\bar{\rho}} \sum_{l=0}^{+\infty} \frac{3}{2l+1} \tilde{p}_l \left(\frac{R}{r} \right)^{l+1} P_l(\cos S) \quad (58)$$

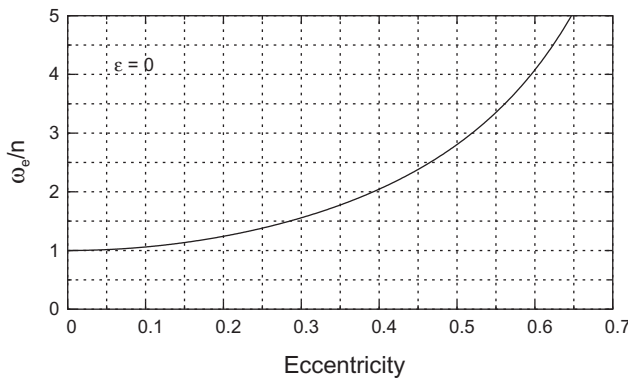


Fig. 4. Evolution of the equilibrium rotation rate $\omega_e/n = f_2(e)/f_1(e)$ with the eccentricity when $\varepsilon = 0^\circ$ using the viscous model (equation (44)). As the eccentricity increases, ω_e also increases.

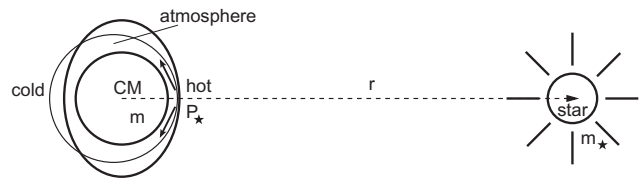


Fig. 5. Thermal atmospheric tides. The atmosphere's heating decreases with the distance to the substellar point P_\star . The atmospheric mass redistribution is essentially decomposed in a weak daily tide (round shape) and in a strong half-daily tide (oval shape).

where $\bar{\rho}$ is the mean density of the planet. Since we are only interested in pressure oscillations, we must subtract the term of constant pressure ($l = 0$) in order to obtain the tidal potential. We also eliminate the diurnal terms ($l = 1$) because they correspond to a displacement of the center of mass of the atmosphere bulge, which has no dynamical implications. Thus, since we usually have $r \gg R$, retaining only the semidiurnal terms ($l = 2$), we write

$$V_a = -\frac{3}{5} \frac{\tilde{p}_2}{\bar{\rho}} \left(\frac{R}{r} \right)^3 P_2(\cos S) \quad (59)$$

2.3.1. Equations of motion. Using the same methodology of previous sections, the contributions of thermal atmospheric tides to the spin evolution are obtained from expression (15) using $U_a = m_\star V_a$ in the place of \bar{U}

$$\frac{d\omega}{dt} = -\frac{3m_\star R^3}{5C\bar{\rho}a^3} \sum_{\sigma} b_a(\sigma) \Omega_{\sigma}^a(x, e) \quad (60)$$

$$\frac{de}{dt} = -\frac{3m_\star R^3}{5C\bar{\rho}a^3} \frac{\sin \varepsilon}{\omega} \sum_{\sigma} b_a(\sigma) E_{\sigma}^a(x, e) \quad (61)$$

where the terms $\Omega_{\sigma}^a(x, e)$ and $E_{\sigma}^a(x, e)$ are also polynomials in the eccentricity, but different from their analogs for gravitational tides (equations (23) and (24)). Nevertheless, when neglecting the terms in e^2 , they become equal and are given by expressions (25) and (26), respectively (with $\tau = a$).

For thermal atmospheric tides there is also a delay before the response of the atmosphere to the excitation (Fig. 6). We name the time delay $\Delta t_a(\sigma)$ and the corresponding phase angle $\delta_a(\sigma)$ (equation (22)). The dissipation factor $b_a(\sigma)$ is given here by

$$b_a(\sigma) = \tilde{p}_2(\sigma) \sin 2\delta_a(\sigma) = \tilde{p}_2(\sigma) \sin(\sigma \Delta t_a(\sigma)) \quad (62)$$

Siebert (1961) and Chapman and Lindzen (1970) have shown that when

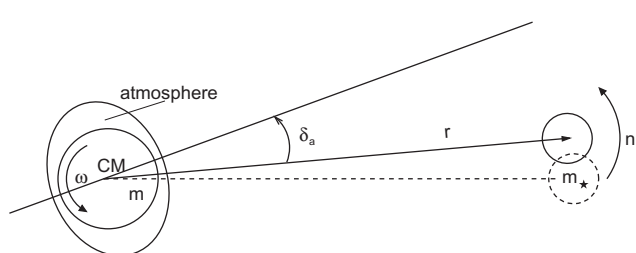


Fig. 6. Phase lag for thermal atmospheric tides. During the time Δt_a the planet turns by an angle $\omega \Delta t_a$ and the star by $n \Delta t_a$. For $\varepsilon = 0$, the bulge phase lag is given by $\delta_a \approx (\omega - n) \Delta t_a$.

$$|\tilde{p}_2(\sigma)| \ll \tilde{p}_0 \quad (63)$$

the amplitudes of the pressure variations on the ground are given by

$$\tilde{p}_2(\sigma) = i \frac{\gamma}{\sigma} \tilde{p}_0 \left(\nabla \cdot \mathbf{v}_{\sigma} - \frac{\gamma - 1}{\gamma} \frac{J_{\sigma}}{gH_0} \right) \quad (64)$$

where $\gamma = 7/5$ for a perfect gas, \mathbf{v} is the velocity of tidal winds, J_{σ} is the amount of heat absorbed or emitted by a unit mass of air per unit time, and H_0 is the scale height at the surface. We can rewrite expression (64) as

$$\begin{aligned} \tilde{p}_2(\sigma) &= \frac{\gamma}{|\sigma|} \tilde{p}_0 \left| \nabla \cdot \mathbf{v}_{\sigma} - \frac{\gamma - 1}{\gamma} \frac{J_{\sigma}}{gH_0} \right| e^{\pm i \frac{\pi}{2}} \\ &= |\tilde{p}_2(\sigma)| e^{\pm i \frac{\pi}{2}} \end{aligned} \quad (65)$$

where the factor $e^{\pm i \frac{\pi}{2}}$ can be seen as a supplementary phase lag of $\pm \pi/2$

$$\begin{aligned} b_a(\sigma) &= |\tilde{p}_2(\sigma)| \sin 2 \left(\delta_a(\sigma) \pm \frac{\pi}{2} \right) \\ &= -|\tilde{p}_2(\sigma)| \sin 2\delta_a(\sigma) \end{aligned} \quad (66)$$

The minus sign above causes pressure variations to lead the Sun whenever $\delta_a(\sigma) < \pi/2$ (Chapman and Lindzen, 1970; Dobrovolskis and Ingersoll, 1980) (Fig. 6).

2.3.2. Dissipation models. Unfortunately, our knowledge of the atmospheric response to thermal excitation is still very incomplete. As for the gravitational tides, models are developed to deal with the unknowns. Dobrovolskis and Ingersoll (1980) adopted a model called “heating at the ground,” where they suppose that all the stellar flux absorbed by the ground F_s is immediately deposited in a thin layer of atmosphere at the surface. The heating distributing may then be written as a δ function just above the ground

$$J(r) = \frac{g}{\tilde{p}_0} F_s \delta(r - 0^+) \quad (67)$$

Neglecting \mathbf{v} over the thin heated layer, expression (64) simplifies as

$$|\tilde{p}_2(\sigma)| = \frac{5}{16} \frac{\gamma - 1}{|\sigma|} \frac{F_s}{H_0} = \frac{5}{16} \frac{\gamma}{|\sigma|} \frac{gF_s}{c_p \bar{T}_s} \quad (68)$$

where the factor $5/16$ represents the second-degree harmonic component of the insolation contribution (Dobrovolskis and Ingersoll, 1980), c_p is the specific heat at constant pressure, and \bar{T}_s the mean surface temperature.

Nevertheless, according to expression (68), if $\sigma = 0$, the amplitude of the pressure variations $\tilde{p}_2(\sigma)$ becomes infinite. The amplitude cannot grow infinitely, as for a tidal frequency equal to zero, a steady distribution is attained. Indeed, expres-

sion (64) is not valid when $\sigma \approx 0$ because condition (63) is no longer verified. Using the typically accepted values for the venusian atmosphere, $c_p \approx 1000 \text{ K kg}^{-1}\text{s}^{-1}$, $\bar{T}_s \approx 730 \text{ K}$, and $F_s \approx 100 \text{ Wm}^{-2}$ (Avduevskii *et al.*, 1976), we compute

$$|\tilde{p}_2(\sigma)| \approx 10^{-4} \tilde{p}_0 \frac{n}{|\sigma|} \quad (69)$$

which means that for $\sigma \sim n$, the “heating at the ground” model of Dobrovolskis and Ingersoll (1980) can still be applied. Since we are only interested in long-term behaviors we can set $\tilde{p}_2(\sigma) = 0$ whenever $|\sigma| \ll n/100$, because for tidal frequencies $\sigma \sim 0$ the dissipation lag $\sin(\sigma\Delta t_a(\sigma)) \approx \sigma\Delta t_a(\sigma)$ also goes to zero. We expect that further studies about the atmospheres of synchronous exoplanets (e.g., Joshi *et al.*, 1997; Arras and Socrates, 2010) may provide a more accurate solution for the case $\sigma \approx 0$.

In the presence of a dense atmosphere, another type of tides can arise: The atmosphere pressure upon the surface gives rise to a deformation, a pressure bulge, that will also be affected by the stellar torque. At the same time, the atmosphere itself exerts a torque over the planet’s bulges (gravitational and pressure bulge). Nevertheless, we do not need to take into account additional tidal effects as their consequences upon the dynamical equations can be neglected (Hinderer *et al.*, 1987; Correia and Laskar, 2003a).

2.4. Spin-Orbit Resonances

A spin-orbit resonance occurs when there is a commensurability between the rotation rate ω and the mean motion of the orbit n (equations (9) and (10)). The synchronous rotation of the Moon is the most common example. After the discovery of the 3/2 spin-orbit resonance of Mercury (Colombo, 1965), spin-orbit resonances were studied in great detail (Colombo and Shapiro, 1966; Goldreich and Peale, 1966; Counselman and Shapiro, 1970; Correia and Laskar, 2004, 2009, 2010). When resonant motion is present we cannot neglect the terms in β in expression (11). Assuming for simplicity a low obliquity ($x \approx 1$), we obtain a nonzero contribution for the rotation rate (equation (16))

$$\frac{d\omega}{dt} = -\beta H(p, e) \sin 2\gamma \quad (70)$$

where $\gamma = \theta - pM - \phi$. The rotation of the planet will therefore present oscillations around a mean value. The width of the corresponding resonance, centered at $\omega = pn$, is

$$\Delta\omega = \sqrt{2\beta H(p, e)} \quad (71)$$

Due to the tidal torque (equation (23)), here denoted by \bar{T} , the mean rotation rate does not remain constant and may therefore cross and be captured in a spin-orbit resonance. Goldreich and Peale (1966) computed a simple estimation of the capture probability P_{cap} , and subsequent more detailed

studies proved their expression to be essentially correct (for a review, see Henrard, 1993). Since the tidal torques can usually be described by means of the torques considered by Goldreich and Peale (1966), we will adopt here the same notations. Let

$$\bar{T} = -K \left(V + \frac{\dot{\gamma}}{n} \right) \quad (72)$$

where K and V are positive constant torques, and $\dot{\gamma} = \omega - pn$. The probability of capture into resonance is then given by (Goldreich and Peale, 1966)

$$P_{\text{cap}} = \frac{2}{1 + \pi Vn / \Delta\omega} \quad (73)$$

where $\Delta\omega$ is the resonance width (equation (71)). In the slow rotation regime ($\omega \sim n$), where the spin encounters spin-orbit resonances and capture may occur, we compute for the viscous tidal model (equation (39))

$$P_{\text{cap}} = 2 \left[1 + \left(p - \frac{2x}{1+x^2} \frac{f_2(e)}{f_1(e)} \right) \frac{n\pi}{2\Delta\omega} \right]^{-1} \quad (74)$$

2.5. Planetary Perturbations

As is the case for planets in the solar system, many exoplanets are not alone in their orbits, but belong to multiplanet systems. Because of mutual planetary perturbations the orbital parameters of the planets do not remain constant and undergo secular variations in time (see chapter by Fabrycky). An important consequence for the spin of the planets is that the reference orbital plane (to which the obliquity and the precession were defined) will also present variations. We can track the orbital plane variations by the inclination to an inertial reference plane, I , and by the longitude of the line of nodes, Ω . Under the assumption of principal axis rotation, the energy perturbation attached to an inertial frame can be written (Kinoshita, 1977; Néron de Surgy and Laskar, 1997)

$$U_{\text{pp}} = \left[X(1 - \cos I) - L \sin \epsilon \sin I \cos \varphi \right] \frac{d\Omega}{dt} + L \sin \epsilon \sin \varphi \frac{dI}{dt} \quad (75)$$

where $\varphi = -\Omega - \psi$.

Although the solar system motion is chaotic (Laskar, 1989, 1990), the motion can be approximated over several million of years by quasiperiodic series. In particular, for the orbital elements that are involved in the precession-driving terms (equation (75)), we have (Laskar and Robutel, 1993)

$$\left(\frac{dI}{dt} + i \frac{d\Omega}{dt} \sin I \right) e^{i\Omega} = \sum_k J_k e^{i(v_k t + \phi_k)} \quad (76)$$

and

$$(1 - \cos I) \frac{d\Omega}{dt} = \sum_k \mathcal{L}_k \cos(v_k t + \phi_k) \quad (77)$$

where v_k are secular frequencies of the orbital motion with amplitude J_k and phase ϕ_k , and $i = \sqrt{-1}$. We may then rewrite expression (75) as

$$\begin{aligned} U_{pp} = & L \sum_k \left[\mathcal{L}_k \cos(v_k t + \phi_k) x \right. \\ & \left. - J_k \sqrt{1-x^2} \sin(v_k t + \psi + \phi_k) \right] \end{aligned} \quad (78)$$

Assuming nonresonant motion, from equations (16) and (17) we get for the spin motion

$$\frac{d\epsilon}{dt} = \sum_k J_k \cos(v_k t + \psi + \phi_k) \quad (79)$$

and

$$\begin{aligned} \frac{d\psi}{dt} = & \alpha \cos \epsilon - \sum_k \mathcal{L}_k \cos(v_k t + \phi_k) \\ & - \cot \epsilon \sum_k J_k \sin(v_k t + \psi + \phi_k) \end{aligned} \quad (80)$$

For planetary systems like the solar system, the mutual inclinations remain small (Laskar, 1990; Correia *et al.*, 2010), and it follows from expressions (76) and (77) that the amplitudes of J_k and \mathcal{L}_k are bounded respectively by

$$J_k \sim v_k I_{\max}, \quad \mathcal{L}_k \sim v_k I_{\max}^2 / 2 \quad (81)$$

The term in \mathcal{L}_k in expression (80) for the precession variations can then be neglected for small inclinations.

From expression (79) it is clear that a resonance can occur whenever the precession frequency is equal to the opposite of a secular frequency v_k (that is, $\dot{\psi} = -v_k$). Retaining only the terms in k , the problem becomes integrable. We can search for the equilibrium positions by setting the obliquity variations equal to zero ($\dot{\epsilon} = 0$). It follows then from expression (79) that $\psi + v_k t + \phi_k = \pm\pi/2$, and replacing it in expression (80) with $\dot{\psi} = -v_k$, we get

$$\alpha \cos \epsilon \sin \epsilon + v_k \sin \epsilon \approx J_k \cos \epsilon \quad (82)$$

which gives the equilibrium positions for the spin of the planet, generally known as “Cassini states” (e.g., Henrard and Murigande, 1987). Since $J_k/v_k \ll 1$ (equation (81)), the equilibrium positions for the obliquity are then

$$\tan \epsilon \approx \frac{J_k}{v_k \pm \alpha}, \quad \cos \epsilon \approx -\frac{v_k}{\alpha} \quad (83)$$

When $|\alpha/v_k| \ll |\alpha/v|_{\text{crit}}$, the first expression gives states 2 and 3, while the second expression has no real roots (states 1

and 4 do not exist). When $|\alpha/v_k| \gg |\alpha/v|_{\text{crit}}$, the first expression approximates Cassini states 1 and 3, while the second one gives states 2 and 4. States 1, 2 and 3 are stable, while state 4 is unstable. Although gravitational tides always decrease the obliquity (equation (45)), the ultimate stage of the obliquity evolution is to be captured into a Cassini resonant state, similar to the capture of the rotation in a spin-orbit resonance (equation (73)).

The complete system (equations (79) and (80)) is usually not integrable as there are several terms in expression (76), but we can look individually to the location of each resonance. When the resonances are far apart, the motion will behave locally as in the integrable case, with the addition of supplementary small oscillations. However, if several resonances overlap, the motion is no longer regular and becomes chaotic (Chirikov, 1979; Laskar, 1996). For instance, the present obliquity variations on Mars are chaotic and can vary from 0° to nearly 60° (Laskar and Robutel, 1993; Touma and Wisdom, 1993; Laskar *et al.*, 2004b).

3. APPLICATION TO THE PLANETS

The orbital parameters of exoplanets are reasonably well determined from radial velocity, transit, or astrometry techniques, but the spins of exoplanets remain a mystery. The same applies to the primordial spins of the terrestrial planets in the solar system, since very few constraints can be derived from the present planetary formation models. Indeed, a small number of large impacts at the end of the formation process will not average, and can change the spin direction. The angular velocities are also unpredictable, but they are usually high, $\omega \gg n$ (Dones and Tremaine, 1993; Agnor *et al.*, 1999; Kokubo and Ida, 2007), although impacts can also form a slow-rotating planet ($\omega \sim n$) if the size of the typical accreting bodies is much smaller than the protoplanet (e.g., Schlichting and Sari, 2007). The critical angular velocity for rotational instability is (Kokubo and Ida, 2007)

$$\omega_{\text{cr}} \approx 3.3 \left(\frac{\rho}{3g \text{ cm}^{-3}} \right)^{1/2} \text{ hr}^{-1} \quad (84)$$

which sets a maximum initial rotation periods of about 1.4 h, for the inner planets of the solar system.

For the jovian planets in the solar system no important mechanism capable of altering the rotation rate is known, but the orientation of the axis may also change by secular resonance with the planets (e.g., Correia and Laskar, 2003b; Ward and Hamilton, 2004; Boué and Laskar, 2010). The fact that all jovian planets rotate fast (Table 3) seems to be in agreement with theoretical predictions (e.g., Takata and Stevenson, 1996).

An empirical relation derived by MacDonald (1964) based on the present rotation rates of planets from Mars to Neptune (assumed almost unchanged) gives for the initial rotation rates

$$\omega_0 \propto m^{4/5} R^{-2} \quad (85)$$

Extrapolating for the remaining inner planets, we get initial rotation periods of about 18.9 h, 13.5 h, and 12.7 h for Mercury, Venus, and Earth, respectively, much faster than today's values, which are in agreement with the present formation theories.

The above considerations and expressions can also be extended to exoplanets. However, since many of the exoplanets are close to their host stars, it is believed that the spins have undergone significant tidal dissipation and eventually reached some equilibrium positions, as happens for Mercury and Venus in the solar system. Therefore, in this section we will first review the rotation of the terrestrial planets, and then look at the already known exoplanets. In particular, we will focus our attention on two classes of exoplanets, the hot Jupiters (fluid) and the super Earths (rocky with atmosphere), for which tidal effects may play an important role in orbital and spin evolution.

3.1. Solar System Examples

3.1.1. Mercury. The present spin of Mercury is very peculiar: The planet rotates three times around its axis in the same time as it completes two orbital revolutions (Pettengill and Dyce, 1965). Within a year of the discovery, the stability of this 3/2 spin-orbit resonance became understood as the result of the solar torque on Mercury's quadrupolar moment of inertia combined with an eccentric orbit (equation (70)) (Colombo and Shapiro, 1966; Goldreich and Peale, 1966). The way the planet evolved into the 3/2 configuration remained a mystery for long time, but can be explained as the result of tidal evolution combined with the eccentricity variations due to planetary perturbations (Correia and Laskar, 2004, 2009). Mercury has no atmosphere, and the spin evolution of the planet is therefore controlled by gravitational tidal interactions with the Sun. Tidal effects drive the final obliquity of Mercury close to zero (equation (45)), and the averaged equation for the rotation motion near the p resonance can be written combining expressions (70) and (39) as

$$\frac{d\omega}{dt} = -\beta' \sin 2\gamma - K' \left[\frac{\omega}{n} - \frac{f_2(e)}{f_1(e)} \right] \quad (86)$$

where $\gamma = \theta - pM - \phi$, $\beta' = \beta H(p, e)$, and $K' = Kn f_1(e)/C$. Note that near the p resonance a contribution from core-mantle friction may also be present, but we will neglect it here (for a full description see Correia and Laskar, 2009, 2010). The tidal equilibrium is achieved when $d\omega/dt = 0$, i.e., for a constant eccentricity e , when $\omega/n = f_2(e)/f_1(e)$. In a circular orbit ($e = 0$) the tidal equilibrium coincides with synchronization, while the equilibrium rotation rate $\omega/n = 3/2$ is achieved for $e_{3/2} = 0.284927$ (Fig. 4).

For the present value of Mercury's eccentricity ($e \approx 0.206$), the capture probability in the 3/2 spin-orbit resonance is only about 7% (equation (74)). However, as the eccentricity of Mercury suffers strong chaotic variations in time due to planetary secular perturbations, the eccentricity

can vary from nearly 0 to more than 0.45, and thus reach values higher than the critical value $e_{3/2} = 0.284927$. Additional capture into resonance can then occur at any time during the planet's history (Correia and Laskar, 2004).

In order to check the past evolution of Mercury's spin, it is not possible to use a single orbital solution; because of the chaotic behavior the motion cannot be predicted precisely beyond a few tens of millions of years. A statistical study of the past evolutions of Mercury's orbit was then performed, with the integration of 1000 orbits over 4 G.y. in the past, starting with very close initial conditions, within the uncertainty of the present determinations (Correia and Laskar, 2004, 2009).

For each of the 1000 orbital motions of Mercury, the rotational motion (equation (86)) was integrated numerically with planetary perturbations. As $e(t)$ is not constant, $\omega(t)$ will tend toward a limit value $\tilde{\omega}(t)$ that is similar to an averaged value of $(f_2/f_1)(e(t))$, and capture into resonance can occur more often (Fig. 7). Globally, only 38.8% of the solutions did not end in resonance, and the final capture probability distribution was (Correia and Laskar, 2004) $P_{1/1} = 2.2\%$, $P_{3/2} = 55.4\%$, $P_{2/1} = 3.6\%$.

With the consideration of the chaotic evolution of the eccentricity of Mercury, the present 3/2 resonant state becomes the most probable outcome for the spin evolution. The largest unknown remains the dissipation factor $k_2 \Delta t$ in the expression of K (equation (43)). A stronger dissipation increases the probability of capture into the 3/2 resonance, as ω/n would follow more closely $f_2(e)/f_1(e)$ (Fig. 7), while lower dissip-

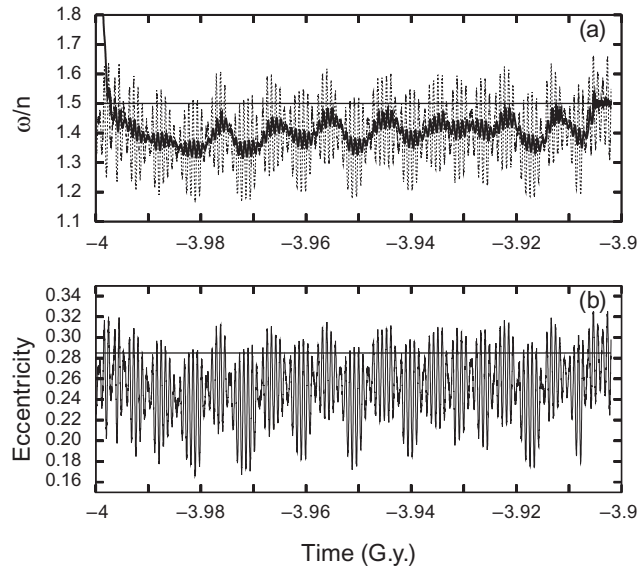


Fig. 7. Simultaneous evolution of (a) the rotation rate and (b) the eccentricity of Mercury. In this example, there is no capture at the first encounter with the 3/2 resonance (at $t \approx -3.9974$ G.y.). About 100 m.y. later, as the mean eccentricity increases, additional crossing of the 3/2 resonance occurs, leading to capture with damping of the libration (Correia and Laskar, 2006).

tion slightly decreases the capture probability. The inclusion of core-mantle friction also increases the chances of capture for all resonances (Correia and Laskar, 2009, 2010).

3.1.2. Venus. Venus is a unique case in the solar system: It presents a slow retrograde rotation, with an obliquity close to 180° and a 243-d period (Smith, 1963; Goldstein, 1964; Carpenter, 1970). According to planetary formation theories it is highly improbable that the present spin of Venus is primordial, since we would expect a lower obliquity and a fast-rotating planet (equation (85)).

The present rotation of Venus is believed to represent a steady state resulting from a balance between gravitational tides, which drives the planet toward synchronous rotation, and thermally driven atmospheric tides, which drives the rotation away (e.g., Gold and Soter, 1969). The conjugated effect of tides and core-mantle friction can tilt Venus down during the planet's past evolution, but requires high values of the initial obliquity (e.g., Dobrovolskis, 1980; Yoder, 1997). However, the crossing in the past of a large chaotic zone for the spin, resulting from secular planetary perturbations (Laskar and Robutel, 1993), can lead Venus to the present retrograde configuration for most initial conditions (Correia and Laskar, 2001, 2003b).

Venus has a dense atmosphere and the planet is also close enough to the Sun to undergo significant tidal dissipation. Venus' spin evolution is then controlled by tidal effects (both gravitational and thermal). Tidal effects combined can drive the obliquity either to $\varepsilon = 0^\circ$ or $\varepsilon = 180^\circ$ (Correia et al., 2003). For the two final obliquity possibilities, the tidal components become very simplified, with (at second order in the planetary eccentricity) a single term of tidal frequency $\sigma = 2\omega - 2n$ for $\varepsilon = 0$ and $\sigma = 2\omega + 2n$ for $\varepsilon = \pi$ (equation (25)). Combining expressions (23) and (60), for the rotation rate we can write

$$\begin{aligned}\frac{d\omega}{dt} \Big|_0 &= -\frac{3}{2} [K_g b_g (2\omega - 2n) + K_a b_a (2\omega - 2n)] \\ \frac{d\omega}{dt} \Big|_\pi &= -\frac{3}{2} [K_g b_g (2\omega + 2n) + K_a b_a (2\omega + 2n)]\end{aligned}\quad (87)$$

where K_g and K_a are given by the constant part of expressions (23) and (60), respectively. Let $f(\sigma)$ be defined as

$$f(\sigma) = \frac{b_a(2\sigma)}{b_g(2\sigma)} \quad (88)$$

As $b_\tau(\sigma)$ is an odd function of σ (equation (25)), $f(\sigma)$ is an even function of σ of the form $f(|\sigma|)$. Thus, at equilibrium, with $d\omega/dt = 0$, we obtain an equilibrium condition

$$f(|\omega - xn|) = -\frac{K_g}{K_a} \quad (89)$$

where $x = +1$ for $\varepsilon = 0$ and $x = -1$ for $\varepsilon = \pi$. Moreover, for all commonly used dissipation models f is monotonic

and decreasing for slow rotation rates. There are thus only four possible values for the final rotation rate ω_f of Venus, given by

$$|\omega - xn| = f^{-1} \left(-\frac{K_g}{K_a} \right) = \omega_s \quad (90)$$

Assuming that the present rotation of Venus corresponds to a stable retrograde rotation, since $\omega_s > 0$ the only possibilities for the present rotation are $\varepsilon = 0$ and $\omega_{obs} = n - \omega_s$, or $\varepsilon = \pi$ and $\omega_{obs} = \omega_s - n$. In both cases, $\omega_s = n + |\omega_{obs}|$ (ω_s is thus the synodic frequency). With

$$\omega_{obs} = 2\pi/243.0185 \text{ day}; \quad n = 2\pi/224.701 \text{ day} \quad (91)$$

we have

$$\omega_s = 2\pi/116.751 \text{ day} \quad (92)$$

We can then determine all four final states for Venus (Table 2). There are two retrograde states (F_0^- and F_π^-) and two prograde states (F_0^+ and F_π^+). The two retrograde states correspond to the observed present retrograde state of Venus with a period of 243.02 d, while the two other states have a prograde rotation period of 76.83 d. Looking to the present rotation state of the planet, it is impossible to distinguish between the two states with the same angular momentum (Fig. 8).

In order to obtain a global view of the possible final evolutions of Venus' spin, numerical integrations of the equations of motion for the dissipative effects (equations (23), (24), (60), and (61)), with the addition of planetary perturbations (equations (79) and (80)), were performed (Correia and Laskar, 2001, 2003b). In Fig. 9 we show the possible final evolutions for a planet starting with an initial period ranging from 3 to 12 d, with an increment of 0.25 d, and initial obliquity from 0° to 180° , with an increment of 2.5° (rotation periods faster than 3 d are excluded as they do not allow the planet to reach a final rotation state within the age of the solar system). Each color represents one of the possible final states. For high initial obliquities, the spin of Venus always evolves into the retrograde final state F_π^- . It is essentially the same evolution as without planetary

TABLE 2. Possible final spin states of Venus.

State	ε	ω	P (days)	P_s (days)
F_0^+	0°	$n + \omega_s$	76.83	116.75
F_0^-	0°	$n - \omega_s$	-243.02	-116.75
F_π^+	180°	$-n - \omega_s$	-76.83	116.75
F_π^-	180°	$-n + \omega_s$	243.02	-116.75

There are two retrograde states (F_0^- and F_π^-) and two prograde states (F_0^+ and F_π^+). In all cases the synodic period P_s is the same (Correia and Laskar, 2001).

perturbations, since none of the trajectories encounters a chaotic zone for the obliquity (Laskar and Robutel, 1993). However, for evolutionary paths starting with low initial obliquities, we can distinguish two different zones: one zone corresponding to slow initial rotation periods ($P_i > 8$ d) where the prograde rotation final state F_0^- is prevailing, and another zone for faster initial rotation periods ($P_i < 8$ d), where we find a mixture of the three attainable final states, F_0^+ , F_0^- , and F_π^- . To emphasize the chaotic behavior, we integrated twice more the zone with $P_i < 8$ d, with a difference of 10^{-9} in the initial eccentricity of Mars (Fig. 9b), and with a difference of 10^{-9} in the initial eccentricity of Neptune (Fig. 9c). The passage through the chaotic zone is reflected by the scattering of the final states in the lefthand side of the figure.

3.1.3. Earth and Mars. Contrary to Mercury and Venus, Earth and Mars are not tidally evolved. For Mars, the tidal

dissipation from the Sun is negligible. For Earth, tidal dissipation is noticeable due to the presence of the Moon, but Earth's spin is still far from the equilibrium (e.g., Néron de Surgy and Laskar, 1997). Nevertheless, the spin axis of both planets is subjected to planetary perturbations and thus present some significant variations (section 2.5).

In the case of Mars, the presence of numerous secular resonances of the kind $\dot{\psi} = -v_k$ (equation (79)) induce large chaotic variations in the obliquity, which can evolve between 0° and 60° (Fig. 10). At present, the obliquity of Mars is very similar to the obliquity of Earth, which is a mere coincidence. Indeed, the obliquity of Mars has most certainly reached values larger than 45° in the past (Laskar et al., 2004a). The periods of high obliquity led to large climatic changes on Mars, with the possible occurrence of large-scale ice cycles where the polar caps are sublimated during high-obliquity stages and the ice is deposited in the equatorial regions (Laskar et al., 2002; Levrard et al., 2004, 2007b).

In the case of Earth, the precession frequency is not in resonance with any orbital secular frequency ($\dot{\psi} \neq v_k$).

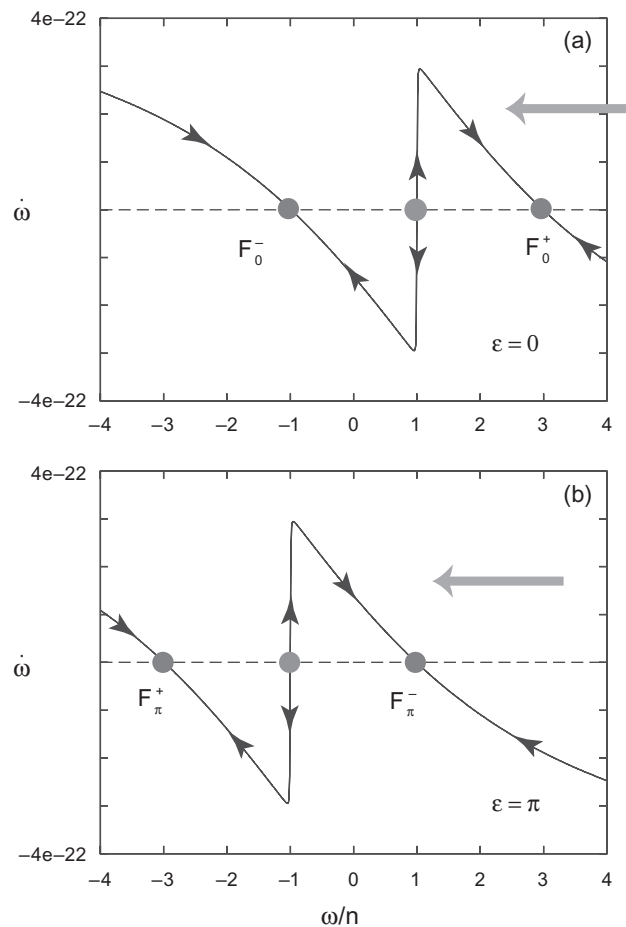


Fig. 8. Final states for a planet with strong atmospheric thermal tides. The original equilibrium point obtained at synchronization ($\omega/n = 1$), when considering uniquely the gravitational tides, becomes unstable, and bifurcates at $\epsilon = 0$ into two new stable fixed points F_0^- and F_0^+ , and at $\epsilon = \pi$ into F_π^- and F_π^+ (Correia and Laskar, 2001, 2003b).

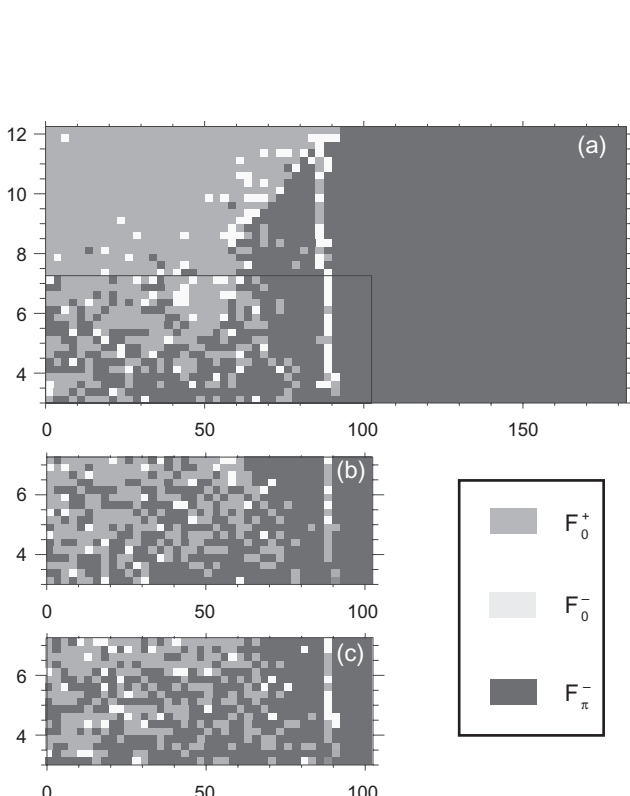


Fig. 9. Final states of Venus' spin with planetary perturbations for initial obliquity [$\epsilon_i \in (0^\circ, 180^\circ)$] and period [$P_i \in (3$ d, 12 d)]. For high initial obliquities, the final evolution of Venus remains essentially unchanged since none of the trajectories crossed the chaotic zone. The passage through the chaotic zone is reflected by the scattering of the final states in the left side of the picture. To emphasize the chaotic behavior, in the bottom left corner of (a), additional integrations were done with the same initial conditions, but with a difference of 10^{-9} in the initial eccentricity of (b) Mars and (c) Neptune (Correia and Laskar, 2003b).

The obliquity of Earth is then only subject to small oscillations of about 1.3° around the mean value (23.3°) with main periodicities around 40,000 yr (Laskar *et al.*, 2004b). The small obliquity variations are nevertheless sufficiently important to induce substantial changes in the insolation received in summer in high-latitude regions on Earth, and they are imprinted in the geological stratigraphic sequences (Hays *et al.*, 1976; Imbrie, 1982).

Due to tidal dissipation in the Earth-Moon system, the Moon is moving away from Earth at a rate of 3.8 cm/yr (Dickey *et al.*, 1994), and the rotation rate of Earth is slowing down (equations (46) and (39), respectively). As a consequence, the torque exerted on the equatorial bulge of Earth decreases and thus the Earth's precession frequency (equations (7) and (12)) as well. Using the present dissipation parameters of Earth, Néron de Surgy and Laskar (1997) found that after 1.5 G.y., the spin of Earth will enter a large chaotic zone of overlapping orbital secular resonances. From then, Earth's spin axis will evolve in a wildly chaotic way, with a possible range from 0° to nearly 90° (Fig. 11).

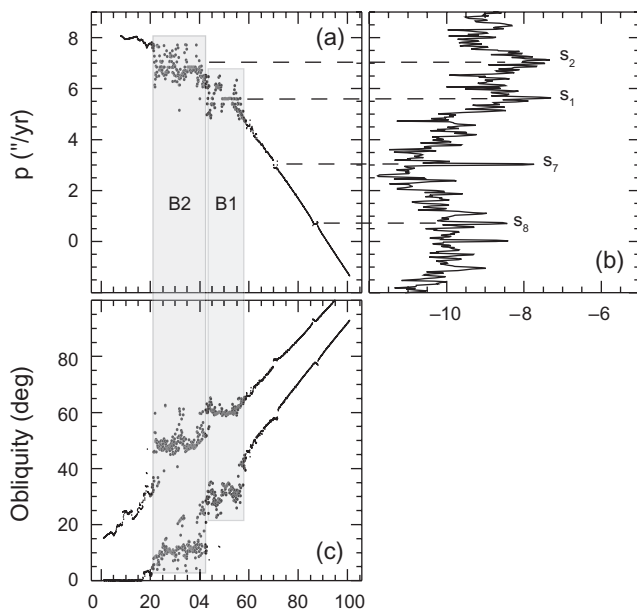


Fig. 10. Frequency analysis of Mars' obliquity. (a) The frequency map is obtained by reporting in the ordinate the value of the precession frequency obtained for 1000 integrations over 56 m.y. for the different values of the initial obliquity (abscissa). A large chaotic zone is visible, ranging from 0° to about 60° , with two distinct zones of large chaos, B1 and B2. (b) Power spectrum of the orbital forcing term (equation (76)) given in logarithmic scale, showing the correspondence of the chaotic zone with the main secular frequencies s_1 , s_2 , s_7 , s_8 (Laskar *et al.*, 2004a). (c) Maximum and minimum values of the obliquity reached over 56 m.y.

The main difference between Earth and Mars is thus due to the presence of the Moon, whose gravitational torque on the equatorial bulge of Earth prevents the spin axis from evolving in a largely chaotic state. Without the presence of the Moon, the behavior of the spin axis of Earth and Mars would be identical (Laskar *et al.*, 1993; Laskar and Robutel, 1993). Depending on the orbital configuration of exoplanetary systems, we thus expect to find planets that would be either in a chaotic state, as Mars or the moonless Earth, or in a regular state, as Earth with the Moon. It should be stressed, however, that the presence of a large satellite is not mandatory in order to stabilize the spin axis. Since the stability of the axis is very important for the exoplanet climate, planetary perturbations should be taken into consideration when searching for other Earth-like environments.

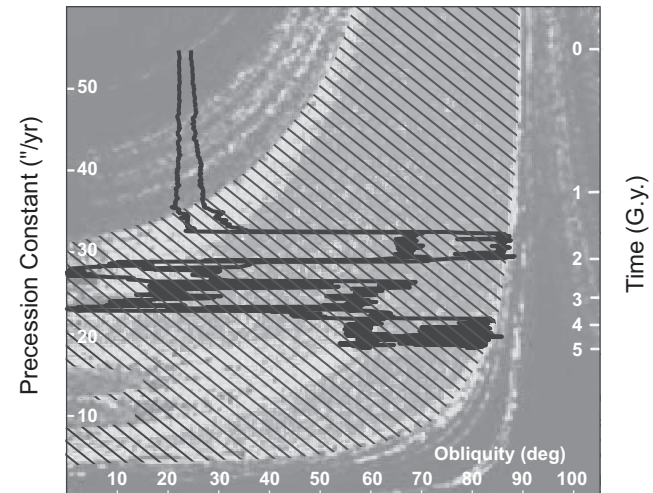


Fig. 11. Example of possible evolution of Earth's obliquity for 5 G.y. in the future, due to tidal dissipation in the Earth-Moon system. The background of the figure is obtained as the result of a stability analysis on about 250,000 numerical integrations of the obliquity of Earth under planetary perturbations for 36 m.y., for various values of the initial obliquity of Earth (x-axis) and various values of the precession constant (left y-axis). We observe a very large chaotic zone (with stripes on the figure) resulting from overlap of orbital secular resonances (Laskar *et al.*, 1993; Laskar and Robutel, 1993). The numerical integration is then conducted over 5 G.y. in the future for the obliquity of Earth, including tidal dissipative effects. The two bold curves correspond to the minimum and maximum values reached by the obliquity and the timescale is given in the right y-axis. As long as the orbits stay in the regular region, the motion suffers only small (and regular) variations. As soon as the orbit enters the chaotic zone, very strong variations of the obliquity are observed, which wanders throughout the chaotic zone, and very high values (close to 90°) are reached (Néron de Surgy and Laskar, 1997).

3.2. Hot Jupiters

One of the most surprising findings concerning exoplanets was the discovery of several giant planets with periods down to 3 d, designated as “hot Jupiters” (e.g., Santos *et al.*, 2005). Many of the hot Jupiters were simultaneously detected by transit method and radial Doppler shift, which allows the direct and accurate determination of both mass and radius of the exoplanet. Therefore, hot Jupiters are among the better characterized planets outside the solar system.

Due to the proximity of the host star, hot Jupiters are almost certainly tidally evolved. Given the large mass of hot Jupiters, they may essentially be composed of an extensive hydrogen atmosphere, similar to Jupiter or Saturn. As a consequence, despite the presence of an inner metallic core, hot Jupiters can be treated as fluid planets, and we may adopt a viscous model for the tidal dissipation (equations (39) and (40)). Thermal atmospheric tides may also be present (e.g., Arras and Socrates, 2010, 2010; Goodman, 2010), but we did not take thermal tides into account, as gravitational tides are so strong for hot Jupiters that they probably rule over all the remaining effects (see section 3.3).

3.2.1. Rotational synchronization. The effect of gravitational tides over the obliquity is to straighten the spin axis (equation (45)), so we will adopt $\epsilon = 0^\circ$ for the obliquity. Assuming that the eccentricity and semimajor axis of the planet are constant, we can derive from expression (39)

$$\frac{\omega}{n} = \frac{f_2(e)}{f_1(e)} + \left(\frac{\omega_0}{n} - \frac{f_2(e)}{f_1(e)} \right) \exp(-t/\tau_{eq}) \quad (93)$$

where $\tau_{eq}^{-1} = Kf_1(e)/C$ is the characteristic timescale for fully despinning the planet.

As for Mercury, the final equilibrium rotation driven by tides ($t \rightarrow +\infty$) is given by the equilibrium position $\omega_e/n = f_2(e)/f_1(e)$, which is different from synchronous rotation if the eccentricity is not zero (Fig. 4). Unlike Mercury, because hot Jupiters are assumed to be fluid, they should not present many irregularities in the internal structures. Therefore $(B-A)/C \approx 0$ and we do not expect hot Jupiters to be captured in spin-orbit resonances. Indeed, determination of second-degree harmonics of the gravity fields of Jupiter and Saturn from Pioneer and Voyager tracking data (Campbell and Anderson, 1989) provided a crude estimate of the $(B-A)/C$ value lower than $\sim 10^{-5}$ for Saturn and $\sim 10^{-7}$ for Jupiter. The $(B-A)/C$ values for Jupiter and Saturn are more than one order of magnitude smaller than the Moon’s or Mercury’s value, leading to insignificant chances of capture. Furthermore, the detection of an equatorial asymmetry is questionable. If an equatorial bulge originates from local mass inhomogeneities driven by convection, it is probably not permanent and must have a more negligible effect if averaged spatially and temporally.

The time required for dampening the rotation of the planet depends on the dissipation factor $k_2\Delta t$ (equation (43)).

Assuming that hot Jupiters are similar to the solar system giant planets, we can adopt $k_2 = 0.4$, and a range for Q from 10^4 to 10^5 (Table 3). The Q factor and the time lag Δt can be related using expressions (22) and (34):

$$Q^{-1} \approx \sigma \Delta t \quad (94)$$

Since we are using a viscous model, for which Δt is made constant, Q will be modified across the evolution as Q is inversely proportional to the tidal frequency σ . The Q factor for the solar system gaseous planets is measured for their present rotation states, which correspond to less than 1 d (Table 3). We may then assume that exoplanets should present identical Q values when they were rotating as rapidly as Jupiter, i.e., $Q_0^{-1} = \omega_0 \Delta t$. For $Q_0 = 10^4$ and $\omega_0 = 2\pi/10$ h, we compute a constant $\Delta t \approx 0.57$ s.

In Fig. 12 we have plotted all known exoplanets, taken from *The Extrasolar Planets Encyclopedia* (<http://exoplanet.eu/>), that could have been tidally evolved. We consider that exoplanets are fully evolved if their rotation rate, starting with an initial period of 10 h, is damped to a value such that $|\omega/n - f_2(e)/f_1(e)| < 0.01$. The curves represent the planets that are tidally evolved in a given time interval ranging from 0.001 G.y. to 10 G.y. Figure 12 allows us to check whether the planet should be fully evolved. For a solar-type star, we can expect that all exoplanets that are above the 1 G.y. curve have already reached the equilibrium rotation ω_e . On the other hand, exoplanets that are below the 10 G.y. curve are probably not yet fully tidally evolved. As expected, all planets in circular orbits with $a < 0.05$ AU are tidally evolved. However, we are more interested in exoplanets further from the star with nonzero eccentricity that are tidally evolved, since the rotation period is not synchronous, but given by expression (44). For instance, for the planet around HD 80606, the orbital period is 111.7 d, but since $e = 0.92$ we predict a rotation period of about 1.9 d.

3.2.2. Cassini states. Until now we have assumed that the final obliquity of the planet is 0° . However, Winn and Holman (2005) suggested that high-obliquity values could be maintained if the planet has been trapped in a Cassini state resonance (equation (82)) since the early despinning process. For small-amplitude variations of the eccentricity

TABLE 3. Constants for the solar system outer planets.

Quantity	Jupiter	Saturn	Uranus	Neptune
$P_0(h)$	9.92	10.66	17.24	16.11
$p(g/cm^3)$	1.33	0.69	1.32	1.64
C/mR^2	0.25	0.21	0.23	0.24
k_2	0.49	0.32	0.36	0.41
$Q (\times 10^4)$	~ 3	~ 2	$1\sim 3$	$1\sim 30$

Data from Yoder (1995); Veverka *et al.* (1994); Dermott *et al.* (1988); Tittemore and Wisdom (1990); Banfield and Murray (1992).

and inclination, the equilibrium positions for the obliquity are given by expression (83). Unless $\alpha = |v_k|$, state 1 is close to 0° , and state 3 is close to 180° . We thus focus only on state 2, which may maintain a significant obliquity.

To test the possibility of capture in the high-obliquity Cassini state 2, we can consider a simple scenario where a hot Jupiter forms at a large orbital distance (approximately several AU) and migrates inward to the current position (~ 0.05 AU). Before the planet reaches typically ~ 0.5 AU, tidal effects do not affect the spin evolution, but the reduction in the semimajor axis increases the precession constant (equation (12)), so that the precession frequency $\dot{\psi}$ may become resonant with some orbital frequencies v_k (equation (80)). The passage through resonance generally causes the obliquity to change (Ward, 1975; Ward and Hamilton, 2004; Hamilton and Ward, 2004; Boué et al., 2009), raising the possibility that the obliquity has a somewhat arbitrary value when the semimajor axis attains ~ 0.5 AU.

Tidal effects become efficient for a < 0.5 AU and drive the obliquity to an equilibrium value $\cos \epsilon \approx 2n(1 + 6e^2)/\omega$ (equation (40)). For initial fast rotation rates ($\omega \gg n$), the equilibrium obliquity tends to 90° . As the rotation rate is decreased by tides, the equilibrium obliquity is reduced to 0° (equation (45)). It is then possible that the obliquity crosses several resonances (one for each frequency v_k) in both ways (increasing and decreasing obliquity), and that a capture occurs. Inside the resonance island, the restoring torque causes the obliquity to librate with amplitude (Correia and Laskar, 2003b)

$$\cos \epsilon_2 \pm \Delta \cos \epsilon_2 \approx -\frac{v_k}{\alpha} \pm 2\sqrt{\frac{J_k}{\alpha}} \sqrt{1 - \frac{v_k^2}{\alpha^2}} \quad (95)$$

Using a linear approximation of the tidal torque (equation (40)) around the resonant obliquity ϵ_2 , the probability of capture in the Cassini state 2 can be estimated from the analytical approach for spin-orbit resonances (equation (73)), with (Levrard et al., 2007a)

$$\frac{\Delta\omega}{\pi V n} = \left[\frac{(1 - 3\cos^2 \epsilon_2)\omega/n + 2\cos \epsilon_2}{\pi \sin^2 \epsilon_2 (2 - \cos \epsilon_2 \omega/n)} \right] \Delta \cos \epsilon_2 \quad (96)$$

In Fig. 13, we plotted the capture probabilities at 0.05, 0.1, and 0.5 AU as a function of the rotation period for different amplitudes (J_k) and frequencies (v_k) characteristic of the solar system (Laskar and Robutel, 1993). As a reasonable example, we choose $v_k = -10''/\text{yr}$, but the results are not affected by changes on this value. Assuming an initial rotation period of 12 h, the capture is possible and even unavoidable if $J_k > 0.1''/\text{yr}$ at 0.5 AU. On the contrary, the chances of capture at 0.05 AU are negligible (<1%) because a decrease in the semimajor axis leads to an increase in the precession constant and reduces the width of the resonance (equation (95)). Theoretical estimations can be compared with numerical simulations (Levrard et al., 2007a). To that

purpose, the spin equations (equations (79) and (80)) were integrated in the presence of tidal effects (equations (39) and (40)) considering 1000 initial precession angles equally distributed over $0-2\pi$ for each initial obliquity. Statistics of capture were found to be in good agreement with previous theoretical estimates.

To test the influence of migration on the capture stability, additional numerical simulations were performed for various initial obliquities and secular perturbations over typically $\sim 5 \times 10^7$ yr. The migration process was simulated by exponentially decreasing the semimajor axis toward 0.05 AU with a 10^5-10^7 yr timescale. The obliquity librations were found to be significantly shorter than spin-down and migration timescales so that the spin trajectory follows an “adiabatic invariant” in the phase space. Nevertheless, expression (40) indicates that the tidal torque dramatically increases with both spin-down and inward migration processes ($d\epsilon/dt \propto a^{-15/2}\omega^{-1}$). If the tidal torque exceeds the maximum possible restoring torque (equation (79)), the resonant equilibrium is destroyed (the evolution is no longer adiabatic). For a given semimajor axis, the stability condition requires then that the rotation rate must always be larger than a threshold value ω_{crit} , which is always verified if $\omega_{\text{crit}} < f_2(e)/f_1(e)$. The stability condition can be simply written as (Levrard et al., 2007a)

$$\tan(\epsilon) < J_k \times \tau_{\text{eq}} \quad (97)$$

where τ_{eq} is the timescale of tidal despinning (equation (93)). It then follows that the final obliquity of the planet cannot be too large, otherwise the planet would quit the resonance.

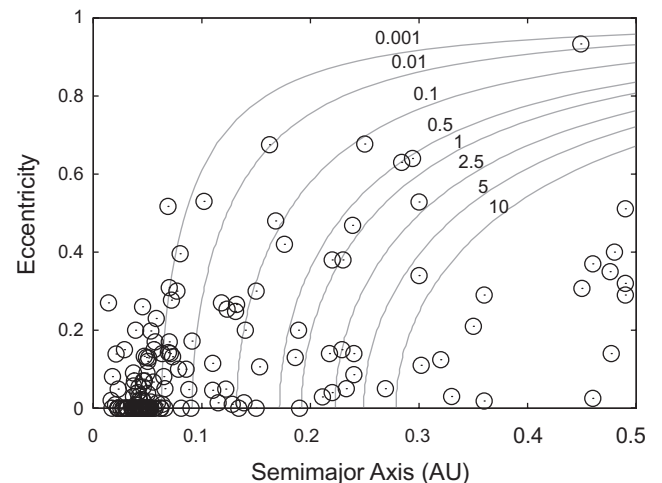


Fig. 12. Tidally evolved exospins with $Q_0 = 10^4$ and initial rotation period $P_0 = 10$ h. The labeled curves denote (in G.y.) the time needed by the rotation to reach the equilibrium (timescales are linearly proportional to Q_0). We assumed Jupiter's geophysical parameters for all planets (Table 3) (updated from Laskar and Correia, 2004).

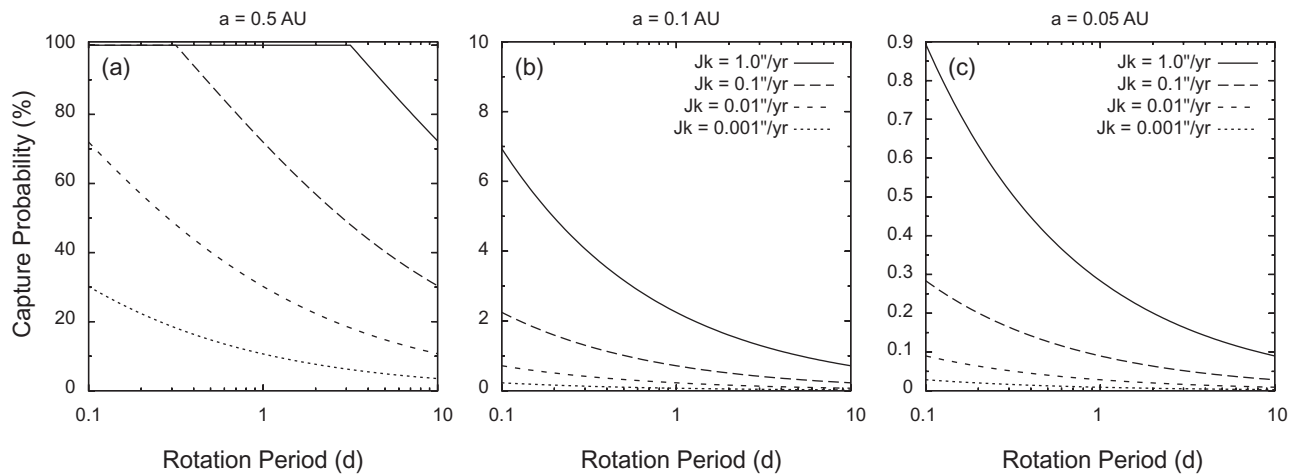


Fig. 13. Obliquity capture probabilities in resonance under the effect of gravitational tides, as a function of the rotation period at (a) 0.5 AU, (b) 0.1 AU, (c) 0.05 AU. J_k is the amplitude of the secular orbital perturbations and $v_k = -10.0''/\text{yr}$ (Levrard *et al.*, 2007a).

For instance, taking $J_k = 1''/\text{yr}$ at 0.05 AU (the highest value in Fig. 13), we need an obliquity $\varepsilon < 21^\circ$. For the more realistic amplitude $J_k = 0.1''/\text{yr}$, the resonant obliquity drops to $\varepsilon < 2^\circ$. Such a low resonant obliquity at 0.05 AU is highly unlikely because, according to expression (83), the resonant state requires very high values of the orbital secular frequencies ($|v_k| > 7.2 \times 10^6''/\text{yr}$). At 0.5 and 0.1 AU, critical obliquity values are respectively 83° and 41° and require more reasonable orbital secular frequencies so that a stable capture is possible. In numerical simulations, the stability criteria for the final obliquity (equation (97)) is empirically retrieved with excellent agreement (Levrard *et al.*, 2007a). When the obliquity leaves the resonance, the obliquity ultimately rapidly switches to the resonant stable Cassini state 1, which tends to 0° (equation (83)). We then conclude that locking a hot Jupiter in an oblique Cassini state seems to be a very unlikely scenario.

3.2.3. Energy balance. Tidal energy is dissipated in the planet at the expense of the rotational and orbital energy so that $\dot{E} = -C\omega\dot{\omega}\cdot\dot{\mathbf{a}}(Gm_\star m)/(2a^2)$. Replacing the equilibrium rotation given by equation (44) in expression (46) we obtain for the tidal energy

$$\dot{E} = Kn^2 \left[f_3(e) - \frac{f_2^2(e)}{f_1(e)} \frac{2x^2}{1+x^2} \right] \quad (98)$$

or, at second order in eccentricity

$$\dot{E} = \frac{Kn^2}{1+\cos^2\varepsilon} \left[\sin^2\varepsilon + e^2(7+16\sin^2\varepsilon) \right] \quad (99)$$

which is always larger than in the synchronous case (e.g., Wisdom, 2004). In Fig. 14 the rate of tidal heating within a nonsynchronous and synchronous planet as a function of the eccentricity ($0 < e < 0.25$) is compared for two different

obliquities (Levrard *et al.*, 2007a). The ratio between the tidal heating in the two situations is an increasing function of both eccentricity and obliquity. For $e \approx 0$, as observed for hot Jupiters, the ratio may reach ~ 1.3 and 2.0 at 45° and 90° obliquity respectively, not being significantly modified at larger eccentricity.

We then conclude that planets in eccentric orbits and/or with high obliquity dissipate more energy than planets in synchronous circular orbits. This may explain why some planets appear to be more inflated than initially expected (e.g., Knutson *et al.*, 2007). A correct tidal energy balance must then take into account the present spin and eccentricity of the orbit.

3.2.4. Orbital circularization. In section 2.2.4 we saw that under tidal friction the spin of the planet attains an equilibrium position faster than the orbit. As a consequence, we can use the expression of the equilibrium rotation rate (equation (44)) in the semimajor axis and eccentricity variations and find simplified expressions (equations (51) and (52)). Combining the two equations we get

$$\frac{da}{a} = \frac{2e de}{(1-e^2)} \quad (100)$$

whose solution is given by

$$a = a_f (1-e^2)^{-1} \quad (101)$$

Replacing the above relation in expression (52) we find a differential equation that rules the eccentricity evolution

$$\dot{e} = -K_0 f_6(e) (1-e^2)^9 e \quad (102)$$

where K_0 is a constant parameter

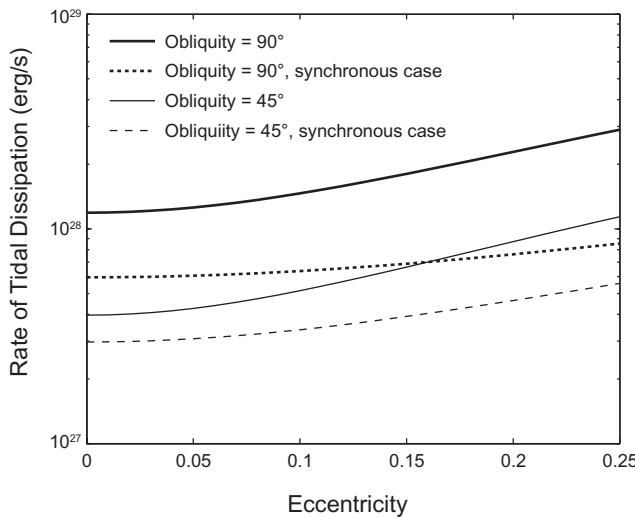


Fig. 14. Rate of tidal dissipation within HD 209458b as a function of the eccentricity for 45° (solid thin line) and 90° (solid thick line) obliquity. The synchronous case is plotted with dashed lines for comparison. The dissipation factor Q_0/k_2 is set to 10^6 (Levrard *et al.*, 2007a).

$$K_0 = \Delta t \frac{21k_2 G m_\star R^5}{2m_f^8} \quad (103)$$

The solution of the above equation is given by

$$F(e) = F(e_0) e^{-K_0 t} \quad (104)$$

where $F(e)$ is an implicit function of e , which converges to zero as $t \rightarrow +\infty$. For small eccentricities, we can neglect terms in e^4 and $F(e) = e|7-9e^2|^{-1/2}$. The characteristic timescale for fully dampening the eccentricity of the orbit is then $\tau_{\text{orb}} \sim 1/K_0$, and the ratio between the spin and orbital timescales

$$\frac{\tau_{\text{eq}}}{\tau_{\text{orb}}} \sim \left(\frac{R}{a_f} \right)^2 \quad (105)$$

Since $a_f = a(1-e^2)$, for initial very eccentric orbits the two timescales become comparable.

In Fig. 15 we have plotted all known exoplanets, taken from *The Extrasolar Planets Encyclopedia* (<http://exoplanet.eu/>), whose orbits could have been tidally evolved. We consider that they are fully evolved if the eccentricity is dampened to a value $e < 0.01$. The curves represent the time needed to damp the eccentricity starting with the present orbital parameters, for time intervals ranging from 0.001 G.y. to 100 G.y. Figure 15 allows us to simultaneously check whether the planet is tidally evolved, and the time needed to fully damp the present eccentricity. All planets in eccentric orbits experience stronger tidal effects because the planet is close to the star at the periape. As a

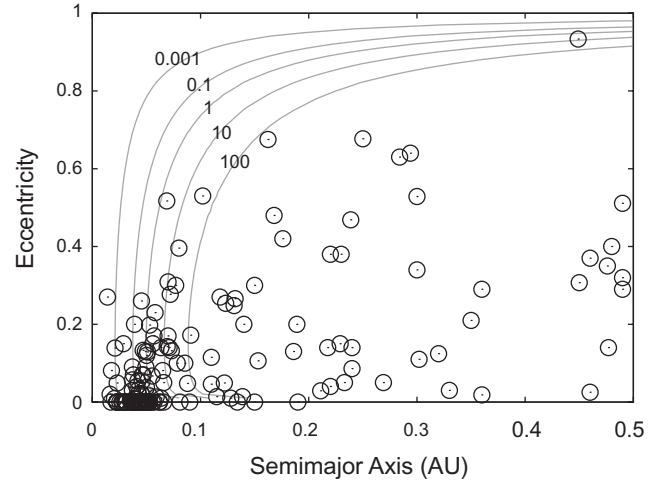


Fig. 15. Tidally evolved orbits of exoplanets with $Q_0 = 10^4$. The labeled curves denote (in G.y.) the time needed to circularize the orbits of the planets ($e < 0.01$) (timescales are linearly proportional to Q_0). We assumed Jupiter's geophysical parameters for all planets (Table 3).

consequence, tidal friction can, under certain conditions, be an important mechanism for the formation of hot Jupiters (see section 3.2.5).

According to Fig. 15, a significant fraction of exoplanets that are close to the host star ($a < 0.1$ AU) still present eccentricities up to 0.4, although tidal effects should have already damped the eccentricity to zero. Observational errors and/or weaker tidal dissipation ($Q_0 \gg 10^4$) can be a possible explanation, but they will hardly justify all the observed situations. A more plausible explanation is that the eccentricity of the exoplanet is being excited by gravitational perturbations from an outer planetary companion (section 2.5). Indeed, the eccentricity of a inner short-period planet can be excited as long as its (nonresonant) outer companion's eccentricity is nonzero. Mardling (2007) has shown that the eccentricity of the outer planet will decay on a timescale that depends on the structure of the inner planet, and that the eccentricities of both planets are damped at the same rate, controlled by the outer planet (Fig. 16). The mechanism is so efficient that the outer planet may be an Earth-mass planet in the “habitable zones” of some stars. As a consequence, the evolution timescale for both eccentricities can be as long as gigayears instead of millions of years, which could explain the current observations of nonzero eccentricity for some hot Jupiters.

3.2.5. Kozai migration. In current theories of planetary formation, the region within 0.1 AU of a protostar is too hot and rarefied for a Jupiter-mass planet to form, so hot Jupiters likely form further away and then migrate inward. A significant fraction of hot Jupiters have been found in systems of binary stars (e.g., Eggenberger *et al.*, 2004), suggesting that the stellar companion may play an important

role in the shrinkage of the planetary orbits. In addition, close binary star systems (separation comparable to the stellar radius) are also often accompanied by a third star. For instance, *Tokovinin et al.* (2006) found that 96% of a sample of spectroscopic binaries with periods less than 3 d have a tertiary component. Indeed, in some circumstances the distant companion enhances tidal interactions in the inner binary, causing the binary orbital period to shrink to the currently observed values. Three-body systems can be stable for long timescales provided that the system is hierarchical, i.e., if the system is formed by an inner binary (star and planet) in a nearly Keplerian orbit with a semimajor axis a , and a outer star also in a nearly Keplerian orbit about the center of mass of the inner system with semimajor axis $a' \gg a$. An additional requirement is that the eccentricity e' of the outer orbit is not too large, in order to prevent close encounters with the inner system. In this situation, perturbations on the inner planetary orbit are weak, but can have important long-term effects (see chapter by Fabrycky).

The most striking effect is known as the Lidov-Kozai mechanism (*Kozai*, 1962; *Lidov*, 1962), which allows the inner orbit to periodically exchange eccentricity with inclination. Even at large distances ($a' > 1000$ AU), the outer star can significantly perturb the planetary orbit as long as the two orbital planes are initially inclined to each other more than $I > 39.2^\circ$ (i.e., for $\cos I < (3/5)^{1/2}$). When $I < 39.2^\circ$ there is little variation in the planet's inclination and eccentricity. Secular effects of the Lidov-Kozai type can then produce large cyclic variations in the planet's eccentricity e as a result of angular momentum exchange with the companion orbit. Since the z component of the planet's angular momentum must be conserved and a is not modified by the secular perturbations, the Kozai integral

$$L_K = (1 - e^2)^{1/2} \cos I \quad (106)$$

is conserved during the oscillations (*Lidov and Ziglin*, 1976). Maxima in e occur with minima in I , and vice versa.

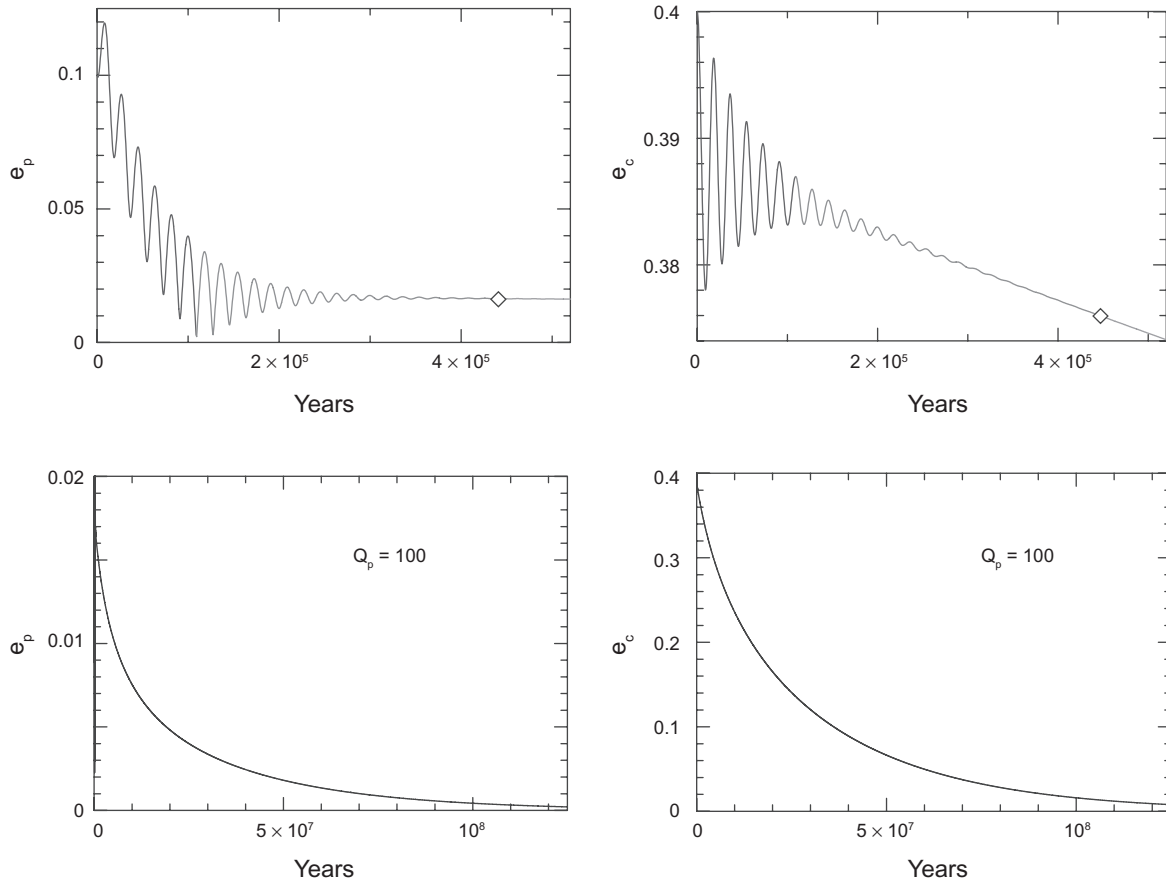


Fig. 16. Tidal evolution of the eccentricities of planet HD 209458b (e_p) perturbed by a $0.1 M_{Jup}$ companion at 0.4 AU (e_c). The dissipation factor $Q_p = 100$ of the observed planet is set artificially low in order to illustrate the damping process (timescales are linearly proportional to Q_p). The top figures show the first stages of the evolution. The change in grayscale shows the transition of the eccentricity from the circulation phase to the libration phase. The diamond represents the moment where the eccentricity librations are damped. Bottom figures show the final evolution of the eccentricities. The result of the presence of a companion is that e_p decays at the same rate as e_c , while the dissipation rate for e_c is controlled by Q_c (*Mardling*, 2007).

If the inner orbit is initially circular, the maximum eccentricity achieved in a Kozai cycle is $e_{\max} = (1 - (5/3) \cos^2 I)^{1/2}$ and the oscillation period of a cycle is approximately P'^2/P (Kiseleva *et al.*, 1998). The maximum eccentricity of the inner orbit in the Kozai cycle will remain fixed for different masses and distances of the outer star, but the period of the Kozai cycle will grow with a'^3 . Kozai cycles persist as long as the perturbation from the outer star is the dominant cause of periape precession in the planetary orbit. However, small additional sources of periape precession such as the quadrupole moments, additional companions, general relativity, or even tides can compensate the Kozai precession and suppress the eccentricity/inclination oscillations (e.g., Migaszewski and Gódziewski, 2009).

Because the Lidov-Kozai mechanism is able to induce large eccentricity excitations, a planet in an initial nearly circular orbit (for instance, a Jupiter-like planet at 5 AU around a Sun-like star) can experience close approaches to the host star at the periape when the eccentricity increases to very high values. As a consequence, tidal effects increase by several orders of magnitude, and according to expression (51) the semimajor axis of the orbit will decrease and the planet migrate inward. At some point of the evolution, the periape precession will be dominated by other effects and the eccentricity oscillations suppressed. From that moment on, the eccentricity is damped according to expression (52) and the final semimajor axis given by $a_f = a(1 - e^2)$. Ford and Rasio (2006) have derived that tidal evolution of high eccentric orbits would end at a semimajor axis a_f equal to about twice the Roche limit R_L . Indeed, at the closest periape distance, attained for $e \approx 1$, we will have $a(1 - e) = R_L$, and thus $a_f = (1 + e)R_L \approx 2R_L$.

In Fig. 17 we plot an example of combined Kozai-tidal migration of the planet HD 80606b. The planet is initially set in an orbit with $a = 5$ AU, $e = 0.1$, and $I = 85.6^\circ$. The stellar companion is supposed to be a Sun-like star at $a' = 1000$ AU, and $e' = 0.5$ (Wu and Murray, 2003; Fabrycky and Tremaine, 2007). Prominent eccentricity oscillations are seen from the very beginning and the energy in the planet's spin is transferred to the orbit, increasing the semimajor axis for the first 0.1 G.y. (equation (39)). As the equilibrium rotation is achieved (equation (44)) the orbital evolution is essentially controlled by equations (51) and (52), whose contributions are enhanced when the eccentricity reaches high values. The semimajor axis evolution is executed by apparent "discontinuous" transitions precisely because the tidal dissipation is only efficient during periods of high eccentricity. As dissipation shrinks the semimajor axis, periape precession becomes gradually dominated by relativity rather than by the third body, and the periape starts circulating as the eccentricity passes close to 0 at 0.7 G.y. Tidal evolution stops when the orbit is completely circularized. The present semimajor axis and eccentricity of planet HD 80606b are $a = 0.45$ AU and $e = 0.92$, respectively, meaning that the tidal evolution on HD 80606b is still underway (Fig. 15). The final semimajor axis is estimated to about $a_f = 0.07$ AU, which corresponds to a regular hot Jupiter.

3.3. Super Earths

After a significant number of discoveries of gaseous giant exoplanets, a new barrier has been passed with the detections of several exoplanets in the Neptune and even Earth-mass (M_\oplus) regime: 2–12 M_\oplus (Rivera *et al.*, 2005; Lovis *et al.*, 2006; Udry *et al.*, 2007; Bonfils *et al.*, 2007); these exoplanets are commonly designated as "super Earths." If the commonly accepted core-accretion model can account for the formation of super Earths, resulting in a mainly icy/rocky composition, the fraction of the residual He-H₂ atmospheric envelope accreted during the planet migration is not tightly constrained for planets more massive than Earth (e.g., Alibert *et al.*, 2006). A minimum mass of below 10 M_\oplus is usually considered to be the boundary between terrestrial and giant planets, but Rafikov (2006) found that planets more massive than 6 M_\oplus could have retained more than 1 M_\oplus of the He-H₂ gaseous envelope. For comparison, masses of Earth's and Venus' atmosphere are respectively $\sim 10^{-6}$ and 10^{-4} times the planet's mass. Despite significant uncertainties, the discoveries of super Earths provide an opportunity to test some properties that could be similar to those of the more familiar terrestrial planets of the solar system.

Because some of the super Earths are potentially in the "habitable zone" (Udry *et al.*, 2007; Selsis *et al.*, 2007), the present spin state is an important factor to constrain the climates. As for Venus, thermal atmospheric tides may have a profound influence on the spin of super Earths. However, the small eccentricity approximation calculated for Venus (equation (87)) may no longer be adequate for super Earths, which exhibit a wide range of eccentricities, orbital distances, or central star types. Although our knowledge of super Earths is restricted to their orbital parameters and minimum masses, we can attempt to place new constraints on the surface rotation rate, assuming that super Earths have a dense atmosphere.

As for Venus, the combined effect of tides is to set the final obliquity at 0° or 180° (Correia *et al.*, 2003). Adopting a viscous dissipation model for tidal effects (equation (37)) and the "heating at the ground" model (Dobrovolskis and Ingersoll, 1980) for surface pressure variations (equation (68)), the average evolution of the rotation rate is then obtained by adding the effects of both tidal torques acting on the planet. From expressions (23) and (60) we get for $\epsilon = 0^\circ$ and to the second order in the eccentricity

$$\frac{\dot{\omega}}{\tau_{\text{eq}}^{-1}} = \omega - (1 + 6e^2)n - \omega_s \left[\left(1 - \frac{21}{2}e^2 \right) \text{sign}(\omega - n) - e^2 \text{sign}(2\omega - n) + 9e^2 \text{sign}(2\omega - 3n) \right] \quad (107)$$

where

$$\omega_s = \frac{F_s}{16H_0k_2} \frac{K_a \Delta t_a}{K_g \Delta t_g} \propto \frac{L_\star}{m_\star} \frac{R}{m} a \quad (108)$$

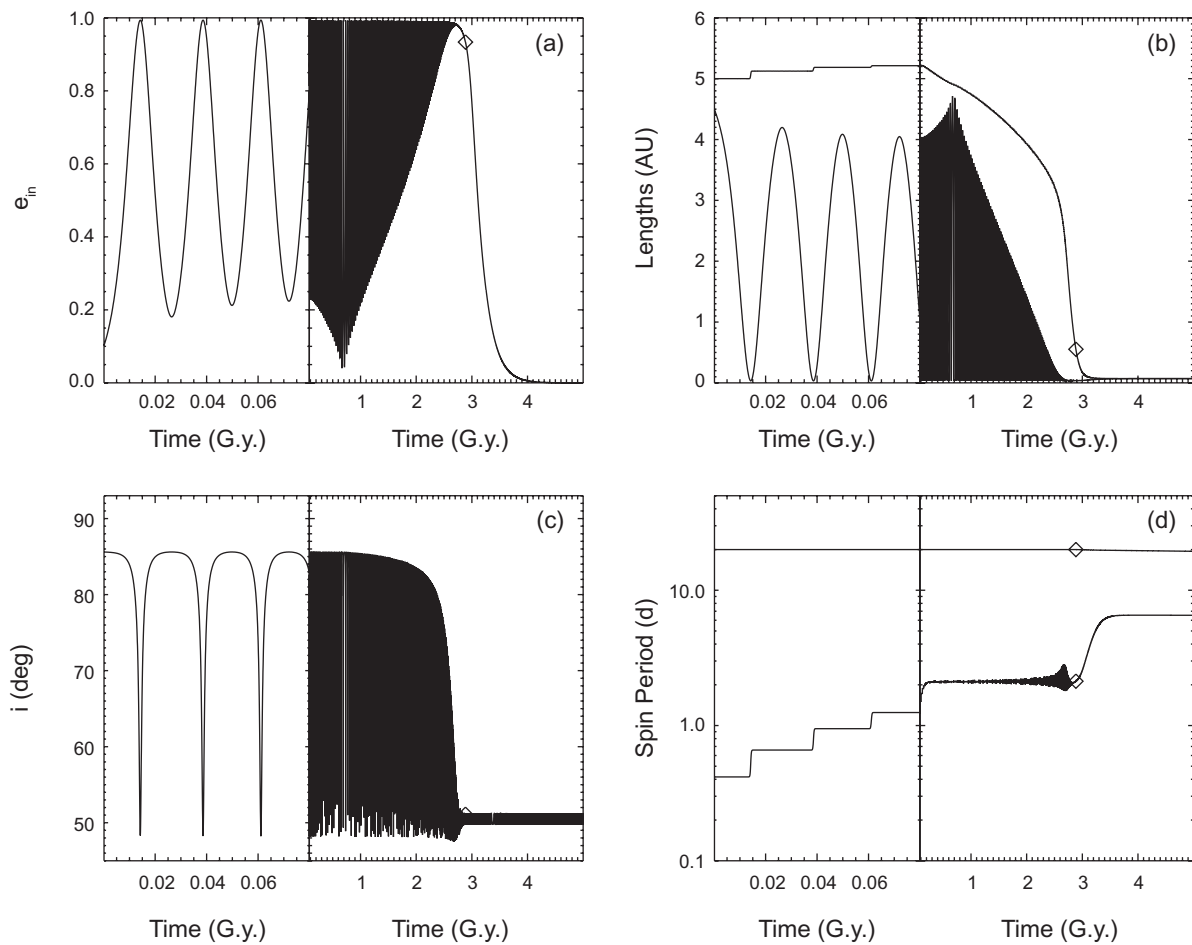


Fig. 17. Possible evolution of the planet HD 80606b initially in an orbit with $a = 5$ AU, $e = 0.1$, and $I = 85.6^\circ$. The stellar companion is supposed to be a Sun-like star at $a' = 1000$ AU, and $e' = 0.5$. The diamonds mark the current position of HD 80606b along this possible evolution (Wu and Murray, 2003; Fabrycky and Tremaine, 2007).

When $e = 0$, we saw in the case of Venus that final positions of the rotation rate at zero obliquity are given by (equation (90))

$$|\omega - n| = \omega_s \quad (109)$$

i.e., there are two final possibilities for the equilibrium rotation of the planet, given by $\omega^\pm = n \pm \omega_s$. When $e \neq 0$, the expression (109) above is no longer valid and additional equilibrium positions for the rotation rate may occur. For moderate values of the eccentricity, from expression (107) we have that the effect of the eccentricity is to eventually split each previous equilibrium rotation rate into two new equilibrium values. Thus, four final equilibrium positions for the rotation rate are possible (eight if we consider the case $\varepsilon = 180^\circ$), obtained with $\dot{\omega} = 0$ (Fig. 18)

$$\omega_{1,2}^\pm = n \pm \omega_s + e^2 \delta_{1,2}^\pm \quad (110)$$

with

$$\delta_1^- = 6n + \frac{1}{2}\omega_s, \quad \delta_1^+ = 6n - \frac{41}{2}\omega_s \quad (111)$$

and

$$\delta_2^- = 6n + \frac{5}{2}\omega_s, \quad \delta_2^+ = 6n - \frac{5}{2}\omega_s \quad (112)$$

Because the set of $\omega_{1,2}^\pm$ values must verify the additional condition

$$\omega_2^- < n/2 < \omega_1^- < n < \omega_1^+ < 3n/2 < \omega_2^+ \quad (113)$$

the four equilibrium rotation states cannot, in general, exist simultaneously, depending on the values of ω_s and e . In particular, the final states ω_1^- and ω_1^+ can never coexist with ω_2^- . At most, three different equilibrium states are therefore possible, obtained when ω_s/n is close to 1/2, or more precisely, when $1/2 - 19e^2/4 < \omega_s/n < 1/2 + 17e^2/4$. Conversely, we find that one single final state $\omega_1^+ = (1 + 6e^2)n + (1 - 41e^2/2)\omega_s$ exists when $\omega_s/n < 6e^2(1 + e^2/2)$.

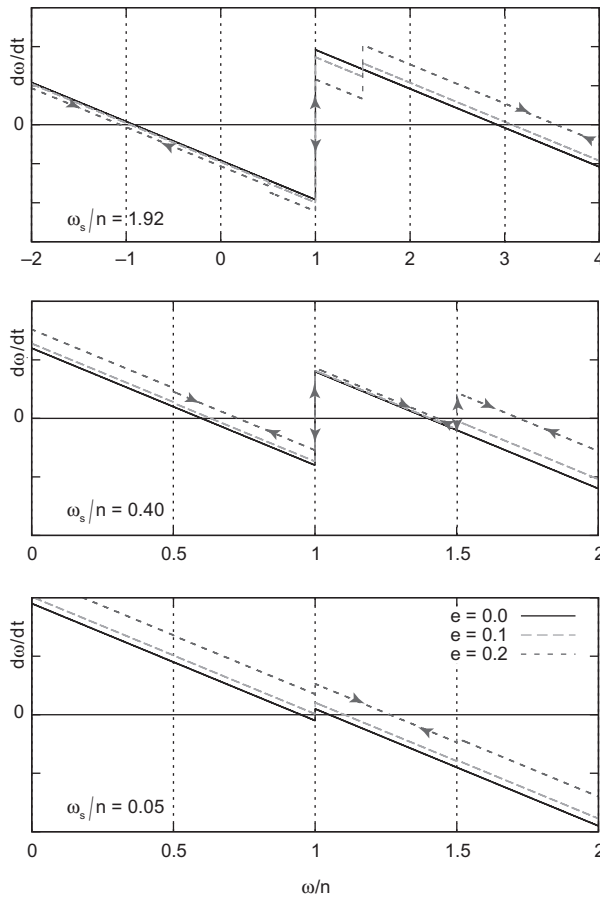


Fig. 18. Evolution of $\dot{\omega}$ (equation (107)) with ω/n for different atmospheric strengths ($\omega_s/n = 1.92, 0.40, 0.05$) and eccentricities ($e = 0.0, 0.1, 0.2$). The top picture with $e = 0$ is the same as Fig. 8 for Venus. The equilibrium rotation rates are given by $\dot{\omega} = 0$ and the arrows indicate whether the equilibrium position is stable or unstable. For $\omega_s/n > 1$, we have two equilibrium possibilities, ω_2^\pm , one of which corresponds to a retrograde rotation (as for Venus). For $\omega_s/n < 1$, retrograde states are not possible, but we can still observe final rotation rates $\omega^- < n$. For eccentric orbits, because of the harmonics in $\sigma = 2\omega - n$ and $\sigma = 2\omega - 3n$, we may have at most four different final possibilities (equation (110)). When ω_s/n becomes extremely small, which is the case for the present observed exoplanets with some eccentricity (Table 4), a single final equilibrium is possible for ω_1^+ (Correia *et al.*, 2008).

Earth and Venus are the only planets that can be included in the category of super Earths for which the atmosphere and spin are known. Only Venus is tidally evolved and therefore suitable for applying the above expressions for tidal equilibrium. We can nevertheless investigate the final equilibrium rotation states of the already detected super Earths. For that purpose, we considered only exoplanets with masses smaller than $12 M_\oplus$ that we classified as rocky planets with a dense atmosphere, although we stress that this mass boundary is quite arbitrary.

Using the empirical mass-luminosity relation $L_\star \propto m_\star^4$ (e.g., Cester *et al.*, 1983) and the mass-radius relationship for terrestrial planets $R \propto m^{0.274}$ (Sotin *et al.*, 2007), expression (108) can be written as

$$\omega_s/n = \kappa (am_\star)^{2.5} m^{-0.726} \quad (114)$$

where κ is a proportionality coefficient that contains all the constant parameters, but also the parameters that we are unable to constrain such as H_0 , k_2 , Δt_g , or Δt_a . In this context, as a first-order approximation we consider that for all super Earths the parameter κ has the same value as for Venus. Assuming that the rotation of Venus is presently stabilized in the ω^- final state, i.e., $2\pi/\omega^- = -243$ d (Carpenter, 1970), we compute $2\pi/\omega_s = 116.7$ d. Replacing the present rotation in expression (114), we find for Venus that $\kappa = 3.723 M_\oplus^{0.726} M_\odot^{-2.5} \text{ AU}^{-2.5}$. We can then estimate the ratio ω_s/n for all considered super Earths in order to derive their respective equilibrium rotation rates (Table 4).

The number and values of the allowed equilibrium rotation states are plotted as a function of am_\star for different eccentricities in Fig. 19. All eccentric planets have a ratio ω_s/n that is lower than 6×10^{-3} (Table 4), which verifies the condition $\omega_s/n < 6e^2(1 + e^2/2)$. As a consequence, only one single final state exists, $\omega_1^+/n \approx (1 + 6e^2)$, corresponding to the equilibrium rotation resulting from gravitational tides (equation (44)). The main reason is that the effect of atmospheric tides is clearly disfavored relative to the effect of gravitational tides on super Earths discovered orbiting M-dwarf stars: The short orbital periods strengthens the effect of gravitational tides, which are proportional to $1/a^6$, while the effect of thermal tides varies as $1/a^5$. Moreover, the small mass of the central star also strongly affects the luminosity received by the planet and hence the size of the atmospheric bulge driven by thermal contrasts.

For the planets with nearly zero eccentricity (GJ 581e, HD 40307b,c,d, and GJ 176b), two equilibrium rotation states ω_1^\pm are possible. However, the two final states ω_1^\pm are so close to the mean motion n , that the quadrupole moment of inertia $(B-A)/C$ will probably capture the rotation of the planet in the synchronous resonance. We then conclude that super Earths orbiting close to their host stars (in particular M dwarfs) will be dominated by gravitational tides and present a final equilibrium rotation rate given by $\omega_e/n \approx f_2(e)/f_1(e)$ (Fig. 4), or present spin-orbit resonances like Mercury.

4. FUTURE PROSPECTS

The classical theory of tides initiated by Darwin (1880, 1908) is sufficient to understand the main effects of tidal friction upon planetary evolution. However, the exact mechanism for how tidal energy is dissipated within the internal layers of the planet remains a challenge for planetary scientists. Kaula (1964) derived a generalization of Darwin's work, with consideration of higher-order tides and without the adoption of any dissipation model. The tidal potential is

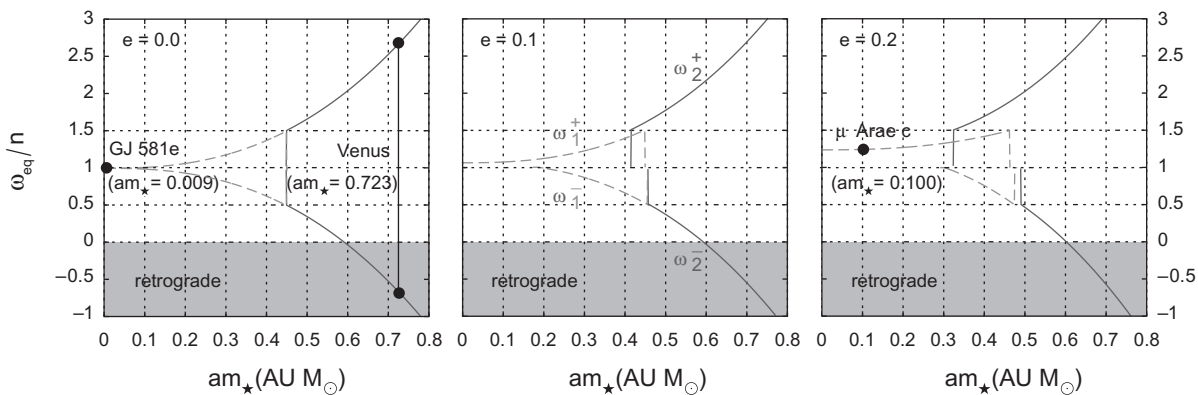


Fig. 19. Equilibrium positions of the rotation rate for super Earths as a function of the product am_{\star} for three different values of the eccentricity ($e = 0.0, 0.1, 0.2$). Each curve corresponds to a different final state (dotted lines for ω_1^{\pm} and solid lines for ω_2^{\pm}). For $e \approx 0$ (case of Venus), we always count two final states that are symmetrical about n . For small values of am_{\star} , the two equilibrium possibilities are so close to n that the most likely scenario for the planet is to be captured in the synchronous resonance (case of GJ 581e). As we increase the eccentricity, we can count at most three final equilibrium rotations, depending on the value of ω/n (computed from equation (114)). When $e \approx 0.2$, only one equilibrium state exists for $am_{\star} < 0.3$, resulting from $\omega/n < 6e^2(1 + e^2/2)$. This is the present situation of μ Arae c and most of the super Earths listed in Table 4 (Correia *et al.*, 2008).

described using infinite series in eccentricity and inclination, which is not practical and can only be correctly handled by computers. Ever since, many efforts have been made in order to either simplify the tidal equations, or to correctly model the tidal dissipation (for a review see Ferraz-Mello *et al.*, 2008; Efroimsky and Williams, 2009). Many solar system phenomena have been successfully explained using the existent tidal models, so we expect that they are suitable to describe the tidal evolution of exoplanets.

Nevertheless, many exoplanets are totally different from the solar system cases, and we cannot exclude the observation of some unexpected behaviors. For instance, it is likely that dissipation within hot Jupiters is closer to dissipation within stars (e.g., Zahn, 1975), while dissipation within super Earths is closer to dissipation observed for rocky planets (e.g., Henning *et al.*, 2009). It is then necessary to continue improving tidal models in order to get a more realistic description for each planetary system. In particular, a correct description of the tidal dissipation and how it evolves with the tidal frequency is critical for the evolution timescale.

The orbital architecture of exoplanetary systems is relatively well determined from the present observational techniques. However, the spins of the exoplanets are not easy to measure, as the lightcurve coming from the planet is always dimmed by the light from the star. The continuous improvements that have been made in photometry and spectrography let us believe that the determination of exoplanets' spins can be a true possibility in the near future. In particular, infrared spectrographs are being developed that will allow acquisition of the spectra of the planets if we manage to subtract the stellar contribution (e.g., Barnes *et al.*, 2010).

Some additional methods for detecting the rotation and

or obliquity of exoplanets have also been tested and suggested so far. For instance, indirect sensing of the planetary gravitational quadrupole and shape, which is linked to both spin rate and obliquity (e.g., Seager and Hui, 2002; Ragozzine and Wolf, 2009), or transient heating of one face of the planet, which then spins into and out of view, has been attempted for the system HD 80606 (Laughlin *et al.*, 2009). The effect of planetary rotation on the transit spectrum of a giant exoplanet is another possibility. During ingress and egress, absorption features arising from the planet's atmosphere are Doppler shifted by a factor on the order of the planet's rotational velocity ($\sim 1-2 \text{ km s}^{-1}$) relative to where they would be if the planet were not rotating (e.g., Spiegel *et al.*, 2007). Finally, for planets whose light is spatially separated from the star, variations may be discernible in the lightcurve obtained by low-precision photometry due to meteorological variability, composition of the surface, or spots (e.g., Ford *et al.*, 2001).

Although the spin states of exoplanets cannot be measured, for exoplanets that are tidally evolved we can still try to make predictions for the rotation rates. When the eccentricity is large, the rotation of many of the observed exoplanets can still be tidally evolved even if the planets are not very close to their central stars (Fig. 12). For tidally evolved hot Jupiters, we can conjecture that the rotation periods are the limit values $P_{\text{orb}} \times f_1(e)/f_2(e)$ (Fig. 4). It becomes a new challenge for the observers to be able to confirm these predictions.

Thermal atmospheric tides may very well destabilize the tidal equilibrium from gravitational tides and create additional possible stable limit values, with the possibility of retrograde rotations, as for planet Venus (Fig. 8).

TABLE 4. Characteristics and equilibrium rotations of some “super Earths” with masses lower than $12 M_{\oplus}$.

Name	Ref.	m_{\star} (M_{\odot})	Age (G.y.)	τ_{eq} (G.y.)	$m \sin i$ (M_{\oplus})	a (AU)	e	ω_s/n	2π/n (d)	2π/ ω_2^- (d)	2π/ ω_1^- (d)	2π/ ω_1^+ (d)	2π/ ω_2^+ (d)
Venus		1.00	4.5	2.3	0.82	0.723	0.007	1.92	224.7	-243.0			76.8
Earth*		1.00	4.5	16	1.00	1.000	0.017	3.75	365.3	-132.9			77.1
GJ 581e	[1]	0.31	7–11	10^{-7}	1.94	0.03	0	10^{-5}	3.4087		3.4088	3.4087	
HD 40307b	[2]	0.77	—	10^{-7}	4.2	0.047	0	0.0003	4.2413		4.2427	4.240	
GJ 581c	[1]	0.31	7–11	10^{-5}	5.36	0.07	0.17	10^{-4}	12.14			10.6335	
GJ 876d	[3]	0.32	9.9	10^{-8}	6.3	0.021	0.14	10^{-6}	1.9649			1.7822	
HD 40307c	[2]	0.77	—	10^{-5}	6.9	0.081	0	0.0009	9.5956		9.6042	9.5871	
GJ 581d	[1]	0.31	7–11	0.02	7.09	0.22	0.38	0.0011	67.6918			47.8226	
HD 181433b	[4]	0.78	—	10^{-5}	7.5	0.08	0.396	0.0008	9.3579			6.535	
GJ 176b	[5]	0.5	—	10^{-5}	8.4	0.066	0	0.0002	8.7583		8.7596	8.7568	
HD 40307d	[2]	0.77	—	10^{-4}	9.2	0.134	0	0.0025	20.4175		20.4696	20.3656	
HD 7924b	[6]	0.83	—	10^{-6}	9.26	0.057	0.17	0.0004	5.4493			4.7688	
HD 69830b	[7]	0.86	4–10	10^{-5}	10.2	0.079	0.10	0.0008	8.6625			8.1995	
μ Arae c	[8]	1.1	6.41	10^{-5}	10.6	0.091	0.172	0.0021	9.5505			8.13313	
55 Cnc e	[9]	1.03	5.5	10^{-7}	10.8	0.038	0.07	0.0002	2.6659			2.592	
GJ 674b	[10]	0.35	0.1–1	10^{-7}	11.09	0.039	0.2	10^{-5}	4.7549			4.0138	
HD 69830c	[7]	0.86	4–10	10^{-3}	11.8	0.186	0.13	0.0064	31.5943			28.8691	

*Moon tidal effects were not included. τ_{eq} was computed with $k_2 = 1/3$ and $\Delta t_g = 640$ s (Earth’s values).

References: [1] Mayor et al. (2009a); [2] Mayor et al. (2009b); [3] Correia et al. (2010); [4] Bouchy et al. (2009); [5] Forveille et al. (2009); [6] Howard et al. (2009); [7] Lovis et al. (2006); [8] Pepe et al. (2007); [9] Fischer et al. (2008); [10] Bonfils et al. (2007).

Thermal tides should be particularly important for super Earths, which are expected to have a distinct rocky body surrounded by a dense atmosphere. In a paradoxical way, the final rotation rate of super Earths are the most difficult to predict, as the equilibrium configurations depend on the composition of the atmospheres. Thermal tides are nevertheless more relevant for exoplanets that orbit Sun-like stars at some distance, like Venus (Fig. 19).

We also assumed that the final obliquity of exoplanets is either 0° or 180° , as the two values represent the final outcome of tidal evolution. However, each planetary system has its own architecture, and planetary perturbations on the spin can lead to resonant capture in high oblique Cassini states or even to chaotic motion. Thus, the final spin evolution of a planet cannot be dissociated from its environment, and a more realistic description of the rotation of exoplanets can only be achieved with the full knowledge of the system orbital dynamics.

Acknowledgments. We thank an anonymous referee for valuable suggestions that helped to improve this work. We acknowledge support from the Fundação para a Ciência e a Tecnologia (Portugal) and PNP-CNRS (France).

REFERENCES

- Abramowitz M. and Stegun I. A. (1972) *Handbook of Mathematical Functions*. Dover, New York.
- Agnor C. B., Canup R. M., and Levison H. F. (1999) On the character and consequences of large impacts in the late stage of terrestrial planet formation. *Icarus*, 142, 219–237.
- Alibert Y., Baraffe I., Benz W., Chabrier G., Mordasini C., Lovis C., Mayor M., Pepe F., Bouchy F., Queloz D., and Udry S. (2006) Formation and structure of the three Neptune-mass planets system around HD 69830. *Astron. Astrophys.*, 455, L25–L28.
- Andoyer H. (1923) *Cours de Mécanique Céleste*. Gauthier-Villars, Paris.
- Arras P. and Socrates A. (2010) Thermal tides in short period exoplanets. *ArXiv e-prints*, arXiv:0901.0735v1.
- Arras P. and Socrates A. (2010) Thermal tides in fluid extrasolar planets. *Astrophys. J.*, 714, 1–12.
- Avduevskii V. S., Golovin I. M., Zavalevich F. S., Likhushin V. I., Marov M. I., Melnikov D. A., Merson I. I., Moshkin B. E., Razin K. A., and Chernoshchekov L. I. (1976) Preliminary results of an investigation of the light regime in the atmosphere and on the surface of Venus. *Kosmich. Issled.*, 14, 735–742.
- Banfield D. and Murray N. (1992) A dynamical history of the inner neptunian satellites. *Icarus*, 99, 390–401.
- Barnes J. R., Barman T. S., Jones H. R. A., Barber R. J., Hansen B. M. S., Prato L., Rice E. L., Leigh C. J., Cameron A. C., and Pinfield D. J. (2010) A search for molecules in the atmosphere of HD 189733b. *Mon. Not. R. Astron. Soc.*, 401, 445–454.
- Bonfils X., Mayor M., Delfosse X., Forveille T., Gillon M., Perrier C., Udry S., Bouchy F., Lovis C., Pepe F., Queloz D., Santos N. C., and Bertaux J.-L. (2007) The HARPS search for southern extra-solar planets. X. A $m \sin i = 11 M_{\oplus}$ planet around the nearby spotted M dwarf GJ 674. *Astron. Astrophys.*, 474, 293–299.
- Bouchy F., Mayor M., Lovis C., Udry S., Benz W., Bertaux J., Delfosse X., Mordasini C., Pepe F., Queloz D., and Segransan D. (2009) The HARPS search for southern extra-solar planets. XVII. Super-Earth and Neptune-mass planets in multiple planet systems HD 47186 and HD 181433. *Astron. Astrophys.*, 496, 527–531.
- Boué G. and Laskar J. (2006) Precession of a planet with a satellite. *Icarus*, 185, 312–330.

- Boué G. and Laskar J. (2010) A collisionless scenario for Uranus tilting. *Astrophys. J. Lett.*, 712, L44–L47.
- Boué G., Laskar J., and Kuchynka P. (2009) Speed limit on Neptune migration imposed by Saturn tilting. *Astrophys. J. Lett.*, 702, L19–L22.
- Brouwer D. and Clemence G. M. (1961) *Methods of Celestial Mechanics*. Academic, New York.
- Campbell J. K. and Anderson J. D. (1989) Gravity field of the saturnian system from Pioneer and Voyager tracking data. *Astron. J.*, 97, 1485–1495.
- Canup R. M. (2005) A giant impact origin of Pluto-Charon. *Science*, 307, 546–550.
- Canup R. M. and Asphaug E. (2001) Origin of the Moon in a giant impact near the end of the Earth’s formation. *Nature*, 412, 708–712.
- Carpenter R. L. (1964) Symposium on radar and radiometric observations of Venus during the 1962 conjunction: Study of Venus by CW radar. *Astron. J.*, 69, 2–11.
- Carpenter R. L. (1970) A radar determination of the rotation of Venus. *Astron. J.*, 75, 61–66.
- Cester B., Ferluga S., and Boehm C. (1983) The empirical mass-luminosity relation. *Astrophys. Space Sci.*, 96, 125–140.
- Chapman S. and Lindzen R. (1970) *Atmospheric Tides: Thermal and Gravitational*. Reidel, Dordrecht.
- Chirikov B. V. (1979) A universal instability of many dimensional oscillator systems. *Phys. Rept.*, 52, 263–379.
- Colombo G. (1965) Rotational period of the planet Mercury. *Nature*, 208, 575–578.
- Colombo G. and Shapiro I. I. (1966) The rotation of the planet Mercury. *Astrophys. J.*, 145, 296–307.
- Correia A. C. M. (2006) The core-mantle friction effect on the secular spin evolution of terrestrial planets. *Earth Planet. Sci. Lett.*, 252, 398–412.
- Correia A. C. M. (2009) Secular evolution of a satellite by tidal effect: Application to Triton. *Astrophys. J. Lett.*, 704, L1–L4.
- Correia A. C. M. and Laskar J. (2001) The four final rotation states of Venus. *Nature*, 411, 767–770.
- Correia A. C. M. and Laskar J. (2003a) Different tidal torques on a planet with a dense atmosphere and consequences to the spin dynamics. *J. Geophys. Res.–Planets*, 108(E11), 5123–10.
- Correia A. C. M. and Laskar J. (2003b) Long-term evolution of the spin of Venus II. Numerical simulations. *Icarus*, 163, 24–45.
- Correia A. C. M. and Laskar J. (2004) Mercury’s capture into the 3/2 spin-orbit resonance as a result of its chaotic dynamics. *Nature*, 429, 848–850.
- Correia A. C. M. and Laskar J. (2006) Evolution of the spin of Mercury and its capture into the 3/2 spin-orbit resonance. In *Past Meets Present in Astronomy and Astrophysics, Proceedings of the 15th Portuguese National Meeting*, pp. 1–4. World Scientific, Singapore.
- Correia A. C. M. and Laskar J. (2009) Mercury’s capture into the 3/2 spin-orbit resonance including the effect of core-mantle friction. *Icarus*, 201, 1–11.
- Correia A. C. M. and Laskar J. (2010) Long-term evolution of the spin of Mercury. I. Effect of the obliquity and core-mantle friction. *Icarus*, 205, 338–355.
- Correia A. C. M., Laskar J., and Néron de Surgy O. (2003) Long-term evolution of the spin of Venus I. Theory. *Icarus*, 163, 1–23.
- Correia A. C. M., Levrard B., and Laskar J. (2008) On the equilibrium rotation of Earth-like extra-solar planets. *Astron. Astrophys.*, 488, L63–L66.
- Correia A. C. M., Couetdic J., Laskar J., Bonfils X., Mayor M., Bertaux J., Bouchy F., Delfosse X., Forveille T., Lovis C., Pepe F., Perrier C., Queloz D., and Udry S. (2010) The HARPS search for southern extra-solar planets. XIX. Characterization and dynamics of the GJ 876 planetary system. *Astron. Astrophys.*, 511, A21.
- Counselman C. C. and Shapiro I. I. (1970) Spin-orbit resonance of Mercury. *Symp. Math.*, 3, 121–169.
- Darwin G. H. (1880) On the secular change in the elements of a satellite revolving around a tidally distorted planet. *Philos. Trans. R. Soc. London*, 171, 713–891.
- Darwin G. H. (1908) *Scientific Papers*. Cambridge Univ., Cambridge.
- Dermott S. F., Malhotra R., and Murray C. D. (1988) Dynamics of the uranus and saturnian satellite systems — A chaotic route to melting Miranda? *Icarus*, 76, 295–334.
- Dickey J. O., Bender P. L., Faller J. E., Newhall X. X., Ricklefs R. L., Ries J. G., Shelus P. J., Veillet C., Whipple A. L., Wiant J. R., Williams J. G., and Yoder C. F. (1994) Lunar laser ranging — a continuing legacy of the Apollo program. *Science*, 265, 482–490.
- Dobrovolskis A. R. (1980) Atmospheric tides and the rotation of Venus. II — Spin evolution. *Icarus*, 41, 18–35.
- Dobrovolskis A. R. and Ingersoll A. P. (1980) Atmospheric tides and the rotation of Venus. I — Tidal theory and the balance of torques. *Icarus*, 41, 1–17.
- Dones L. and Tremaine S. (1993) On the origin of planetary spins. *Icarus*, 103, 67–92.
- Efroimsky M. and Williams J. G. (2009) Tidal torques: A critical review of some techniques. *Cel. Mech. Dyn. Astron.*, 104, 257–289.
- Eggenberger A., Udry S., and Mayor M. (2004) Statistical properties of exoplanets. III. Planet properties and stellar multiplicity. *Astron. Astrophys.*, 417, 353–360.
- Escribano B., Vanyo J., Tuval I., Cartwright J. H. E., González D. L., Piro O., and Tél T. (2008) Dynamics of tidal synchronization and orbit circularization of celestial bodies. *Phys. Rev.*, E78(3), 036216.
- Fabrycky D. and Tremaine S. (2007) Shrinking binary and planetary orbits by Kozai cycles with tidal friction. *Astrophys. J.*, 669, 1298–1315.
- Ferraz-Mello S., Rodríguez A., and Hussmann H. (2008) Tidal friction in close-in satellites and exoplanets: The Darwin theory re-visited. *Cel. Mech. Dyn. Astron.*, 101, 171–201.
- Fischer D. A., Marcy G. W., Butler R. P., Vogt S. S., Laughlin G., Henry G. W., Abouav D., Peek K. M. G., Wright J. T., Johnson J. A., McCarthy C., and Isaacson H. (2008) Five planets orbiting 55 Cancri. *Astrophys. J.*, 675, 790–801.
- Ford E. B. and Rasio F. A. (2006) On the relation between hot Jupiters and the Roche limit. *Astrophys. J. Lett.*, 638, L45–L48.
- Ford E. B., Seager S., and Turner E. L. (2001) Characterization of extrasolar terrestrial planets from diurnal photometric variability. *Nature*, 412, 885–887.
- Forveille T., Bonfils X., Delfosse X., Gillon M., Udry S., Bouchy F., Lovis C., Mayor M., Pepe F., Perrier C., Queloz D., Santos N., and Bertaux J.-L. (2009) The HARPS search for southern extra-solar planets. XIV. Gl 176b, a super-Earth rather than a Neptune, and at a different period. *Astron. Astrophys.*, 493, 645–650.
- Gold T. and Soter S. (1969) Atmospheric tides and the resonant rotation of Venus. *Icarus*, 11, 356–366.
- Goldreich P. and Peale S. (1966) Spin-orbit coupling in the solar system. *Astron. J.*, 71, 425–438.

- Goldreich P. and Peale S. J. (1968) The dynamics of planetary rotations. *Annu. Rev. Astron. Astrophys.*, 6, 287–320.
- Goldreich P. and Soter S. (1966) Q in the solar system. *Icarus*, 5, 375–389.
- Goldreich P., Murray N., Longaretti P. Y., and Banfield D. (1989) Neptune's story. *Science*, 245, 500–504.
- Goldstein H. (1950) *Classical Mechanics*. Addison-Wesley, Reading.
- Goldstein R. M. (1964) Symposium on radar and radiometric observations of Venus during the 1962 conjunction: Venus characteristics by Earth-based radar. *Astron. J.*, 69, 12–19.
- Goodman J. (2010) Concerning thermal tides on hot Jupiters. *ArXiv e-prints*, arXiv:0901.3279v1.
- Hamilton D. P. and Ward W. R. (2004) Tilting Saturn. II. Numerical model. *Astron. J.*, 128, 2510–2517.
- Hays J. D., Imbrie J., and Shackleton N. J. (1976) Variations in the Earth's orbit: Pacemaker of the ice ages. *Science*, 194, 1121–1132.
- Henning W. G., O'Connell R. J., and Sasselov D. D. (2009) Tidally heated terrestrial exoplanets: Viscoelastic response models. *Astrophys. J.*, 707, 1000–1015.
- Henrard J. (1993) The adiabatic invariant in classical dynamics. In *Dynamics Reported*, pp. 117–235. Springer Verlag, New York.
- Henrard J. and Murigande C. (1987) Colombo's top. *Cel. Mech.*, 40, 345–366.
- Hinderer J., Legros H., and Pedotti G. (1987) Atmospheric pressure torque and axial rotation of Venus. *Adv. Space Res.*, 7, 311–314.
- Howard A. W., Johnson J. A., Marcy G. W., Fischer D. A., Wright J. T., Henry G. W., Giguere M. J., Isaacson H., Valenti J. A., Anderson J., and Piskunov N. E. (2009) The NASA-UC Etat-Earth Program. I. A super-Earth orbiting HD 7924. *Astrophys. J.*, 696, 75–83.
- Imbrie J. (1982) Astronomical theory of the Pleistocene ice ages — A brief historical review. *Icarus*, 50, 408–422.
- Jones H. R. A., Butler R. P., Tinney C. G., Marcy G. W., Carter B. D., Penny A. J., McCarthy C., and Bailey J. (2006) High-eccentricity planets from the Anglo-Australian Planet Search. *Mon. Not. R. Astron. Soc.*, 369, 249–256.
- Joshi M. M., Haberle R. M., and Reynolds R. T. (1997) Simulations of the atmospheres of synchronously rotating terrestrial planets orbiting M dwarfs: Conditions for atmospheric collapse and the implications for habitability. *Icarus*, 129, 450–465.
- Kaula W. M. (1964) Tidal dissipation by solid friction and the resulting orbital evolution. *Rev. Geophys.*, 2, 661–685.
- Kinoshita H. (1977) Theory of the rotation of the rigid Earth. *Cel. Mech.*, 15, 277–326.
- Kiseleva L. G., Eggleton P. P., and Mikkola S. (1998) Tidal friction in triple stars. *Mon. Not. R. Astron. Soc.*, 300, 292–302.
- Knutson H. A., Charbonneau D., Noyes R. W., Brown T. M., and Gilliland R. L. (2007) Using stellar limb-darkening to refine the properties of HD 209458b. *Astrophys. J.*, 655, 564–575.
- Kokubo E. and Ida S. (2007) Formation of terrestrial planets from protoplanets. II. Statistics of planetary spin. *Astrophys. J.*, 671, 2082–2090.
- Kozai Y. (1962) Secular perturbations of asteroids with high inclination and eccentricity. *Astron. J.*, 67, 591–598.
- Lambeck K. (1980) *The Earth's Variable Rotation: Geophysical Causes and Consequences*. Cambridge Univ., Cambridge.
- Laskar J. (1989) A numerical experiment on the chaotic behaviour of the solar system. *Nature*, 338, 237–238.
- Laskar J. (1990) The chaotic motion of the solar system — A numerical estimate of the size of the chaotic zones. *Icarus*, 88, 266–291.
- Laskar J. (1996) Large scale chaos and marginal stability in the solar system. *Cel. Mech. Dyn. Astron.*, 64, 115–162.
- Laskar J. and Correia A. C. M. (2004) The rotation of extra-solar planets. In *Extrasolar Planets: Today and Tomorrow* (J.-P. Beauville et al., eds.), pp. 401–409. ASP Conf. Ser. 321, Astronomical Society of the Pacific, San Francisco.
- Laskar J. and Robutel P. (1993) The chaotic obliquity of the planets. *Nature*, 361, 608–612.
- Laskar J., Joutel F., and Robutel P. (1993) Stabilization of the Earth's obliquity by the Moon. *Nature*, 361, 615–617.
- Laskar J., Levrard B., and Mustard J. F. (2002) Orbital forcing of the martian polar layered deposits. *Nature*, 419, 375–377.
- Laskar J., Correia A. C. M., Gastineau M., Joutel F., Levrard B., and Robutel P. (2004a) Long term evolution and chaotic diffusion of the insolation quantities of Mars. *Icarus*, 170, 343–364.
- Laskar J., Robutel P., Joutel F., Gastineau M., Correia A. C. M., and Levrard B. (2004b) A long-term numerical solution for the insolation quantities of the Earth. *Astron. Astrophys.*, 428, 261–285.
- Laughlin G., Deming D., Langton J., Kasen D., Vogt S., Butler P., Rivera E., and Meschiari S. (2009) Rapid heating of the atmosphere of an extrasolar planet. *Nature*, 457, 562–564.
- Levrard B., Forget F., Montmessin F., and Laskar J. (2004) Recent ice-rich deposits formed at high latitudes on Mars by sublimation of unstable equatorial ice during low obliquity. *Nature*, 431, 1072–1075.
- Levrard B., Correia A. C. M., Chabrier G., Baraffe I., Selsis F., and Laskar J. (2007a) Tidal dissipation within hot Jupiters: A new appraisal. *Astron. Astrophys.*, 462, L5–L8.
- Levrard B., Forget F., Montmessin F., and Laskar J. (2007b) Recent formation and evolution of northern martian polar layered deposits as inferred from a global climate model. *J. Geophys. Res.—Planets*, 112(E11), 6012.
- Lidov M. L. (1962) The evolution of orbits of artificial satellites of planets under the action of gravitational perturbations of external bodies. *Planet. Space Sci.*, 9, 719–759.
- Lidov M. L. and Ziglin S. L. (1976) Non-restricted double-averaged three body problem in Hill's case. *Cel. Mech.*, 13, 471–489.
- Lois C., Mayor M., Pepe F., Alibert Y., Benz W., Bouchy F., Correia A. C. M., Laskar J., Mordasini C., Queloz D., Santos N. C., Udry S., Bertaux J.-L., Sivan J.-P., (2006) An extrasolar planetary system with three Neptune-mass planets. *Nature*, 441, 305–309.
- MacDonald G. J. F. (1964) Tidal friction. *Rev. Geophys.*, 2, 467–541.
- Mardling R. A. (2007) Long-term tidal evolution of short-period planets with companions. *Mon. Not. R. Astron. Soc.*, 382, 1768–1790.
- Mayor M., Bonfils X., Forveille T., Delfosse X., Udry S., Bertaux J., Beust H., Bouchy F., Lovis C., Pepe F., Perrier C., Queloz D., and Santos N. C. (2009a) The HARPS search for southern extra-solar planets. XVIII. An Earth-mass planet in the GJ 581 planetary system. *Astron. Astrophys.*, 507, 487–494.
- Mayor M., Udry S., Lovis C., Pepe F., Queloz D., Benz W., Bertaux J.-L., Bouchy F., Mordasini C., and Segransan D. (2009b) The HARPS search for southern extra-solar planets. XIII. A planetary system with 3 super-Earths (4.2, 6.9, and 9.2 M_⊕). *Astron. Astrophys.*, 493, 639–644.
- Migaszewski C. and Gózdziewski K. (2009) Secular dynamics of

- a coplanar, non-resonant planetary system under the general relativity and quadrupole moment perturbations. *Mon. Not. R. Astron. Soc.*, 392, 2–18.
- Mignard F. (1979) The evolution of the lunar orbit revisited. I. *Moon Planets*, 20, 301–315.
- Mignard F. (1980) The evolution of the lunar orbit revisited. II. *Moon Planets*, 23, 185–201.
- Mignard F. (1981) Evolution of the martian satellites. *Mon. Not. R. Astron. Soc.*, 194, 365–379.
- Munk W. H. and MacDonald G. J. F. (1960) *The Rotation of the Earth; A Geophysical Discussion*. Cambridge Univ., Cambridge.
- Murray C. D. and Dermott S. F. (1999) *Solar System Dynamics*. Cambridge Univ., Cambridge.
- Naef D., Latham D. W., Mayor M., Mazeh T., Beuzit J. L., Drukier G. A., Perrier-Bellet C., Queloz D., Sivan J. P., Torres G., Udry S., and Zucker S. (2001) HD 80606b, a planet on an extremely elongated orbit. *Astron. Astrophys.*, 375, L27–L30.
- Néron de Surgy O. and Laskar J. (1997) On the long term evolution of the spin of the Earth. *Astron. Astrophys.*, 318, 975–989.
- Pepe F., Correia A. C. M., Mayor M., Tamuz O., Couetdic J., Benz W., Bertaix J.-L., Bouchy F., Laskar J., Lovis C., Naef D., Queloz D., Santos N. C., Sivan J.-P., Sosnowska D., and Udry S. (2007) The HARPS search for southern extra-solar planets. VIII. μ Arae, a system with four planets. *Astron. Astrophys.*, 462, 769–776.
- Pettengill G. H. and Dyce R. B. (1965) A radar determination of the rotation of the planet Mercury. *Nature*, 206, 1240–1241.
- Rafikov R. R. (2006) Atmospheres of protoplanetary cores: Critical mass for nucleated instability. *Astrophys. J.*, 648, 666–682.
- Ragozzine D. and Wolf A. S. (2009) Probing the interiors of very hot Jupiters using transit light curves. *Astrophys. J.*, 698, 1778–1794.
- Rivera E. J., Lissauer J. J., Butler R. P., Marcy G. W., Vogt S. S., Fischer D. A., Brown T. M., Laughlin G., and Henry G. W. (2005) A $\sim 7.5 M_{\oplus}$ planet orbiting the nearby star, GJ 876. *Astrophys. J.*, 634, 625–640.
- Santos N. C., Benz W., and Mayor M. (2005) Extrasolar planets: Constraints for planet formation models. *Science*, 310, 251–255.
- Schiaparelli G. V. (1889) Sulla rotazione di Mercurio. *Astronom. Nach.*, 123, 241–250.
- Schlichting H. E. and Sari R. (2007) The effect of semicollisional accretion on planetary spins. *Astrophys. J.*, 658, 593–597.
- Seager S. and Hui L. (2002) Constraining the rotation rate of transiting extrasolar planets by oblateness measurements. *Astrophys. J.*, 574, 1004–1010.
- Selsis F., Kasting J., Levrard B., Paillet J., Ribas I., and Delfosse X. (2007) Habitable planets around the star Gliese 581? *Astron. Astrophys.*, 476, 1373–1387.
- Siebert M. (1961) Atmospheric tides. *Adv. Geophys.*, 7, 105–187.
- Smart W. M. (1953) *Celestial Mechanics*. London, New York.
- Smith W. B. (1963) Radar observations of Venus, 1961 and 1959. *Astron. J.*, 68, 15–21.
- Sotin C., Grasset A., and Mocquet A. (2007) Mass-radius curve for extrasolar Earth-like planets and ocean planets. *Icarus*, 191, 337–351.
- Spiegel D. S., Haiman Z., and Gaudi B. S. (2007) On constraining a transiting exoplanet's rotation rate with its transit spectrum. *Astrophys. J.*, 669, 1324–1335.
- Takata T. and Stevenson D. J. (1996) Despin mechanism for protogiant planets and ionization state of protogiant planetary disks. *Icarus*, 123, 404–421.
- Tamuz O., Ségransan D., Udry S., Mayor M., Eggenberger A., Naef D., Pepe F., Queloz D., Santos N. C., Demory B., Figuera P., Marmier M., and Montagnier G. (2008) The CORALIE survey for southern extrasolar planets. XV. Discovery of two eccentric planets orbiting HD 4113 and HD 156846. *Astron. Astrophys.*, 480, L33–L36.
- Tisserand F. (1891) *Traité de Mécanique Céleste (Tome II)*. Gauthier-Villars, Paris.
- Tittemore W. C. and Wisdom J. (1990) Tidal evolution of the uranusian satellites. III — Evolution through the Miranda-Umbriel 3:1, Miranda-Ariel 5:3, and Ariel-Umbriel 2:1 mean-motion commensurabilities. *Icarus*, 85, 394–443.
- Tokovinin A., Thomas S., Sterzik M., and Udry S. (2006) Tertiary companions to close spectroscopic binaries. *Astron. Astrophys.*, 450, 681–693.
- Touma J. and Wisdom J. (1993) The chaotic obliquity of Mars. *Science*, 259, 1294–1297.
- Udry S., Bonfils X., Delfosse X., Forveille T., Mayor M., Perrier C., Bouchy F., Lovis C., Pepe F., Queloz D., and Bertaix J.-L. (2007) The HARPS search for southern extra-solar planets. XI. Super-Earths (5 and $8 M_{\oplus}$) in a 3-planet system. *Astron. Astrophys.*, 469, L43–L47.
- Veeder G. J., Matson D. L., Johnson T. V., Blaney D. L., and Goguen J. D. (1994) Io's heat flow from infrared radiometry: 1983–1993. *J. Geophys. Res.*, 99, 17095–17162.
- Ward W. R. (1975) Tidal friction and generalized Cassini's laws in the solar system. *Astron. J.*, 80, 64–70.
- Ward W. R. and Hamilton D. P. (2004) Tilting Saturn. I. Analytic model. *Astron. J.*, 128, 2501–2509.
- Williams G. E. (1990) Precambrian cyclic rhythmites: Solar-climatic or tidal signatures? *Phil. Trans. R. Soc. London A*, 330, 445–457.
- Winn J. N. and Holman M. J. (2005) Obliquity tides on hot Jupiters. *Astrophys. J. Lett.*, 628, L159–L162.
- Wisdom J. (2004) Spin-orbit secondary resonance dynamics of Enceladus. *Astron. J.*, 128, 484–491.
- Wisdom J., Peale S. J., and Mignard F. (1984) The chaotic rotation of Hyperion. *Icarus*, 58, 137–152.
- Wu Y. and Murray N. (2003) Planet migration and binary companions: The Case of HD 80606b. *Astrophys. J.*, 589, 605–614.
- Yoder C. F. (1995) Venus' free obliquity. *Icarus*, 117, 250–286.
- Yoder C. F. (1997) Venusian spin dynamics. In *Venus II — Geology, Geophysics, Atmosphere, and Solar Wind Environment* (S. W. Bougher et al., eds.), pp. 1087–1124. Univ. of Arizona, Tucson.
- Zahn J. (1975) The dynamical tide in close binaries. *Astron. Astrophys.*, 41, 329–344.